

Optimization of baseload electricity and hydrogen services by renewables for a nuclear-sized district in South Italy

Luigi Moccia*

June 28, 2024

Abstract

We present an optimization model of an energy district in South Italy that supplies baseload electricity and hydrogen services. The district is sized such that a nuclear reactor could provide these services. We define scenarios for 2050 to explore the system effects of discount rate sensitivity and vetoes on technologies. We address the following issues relevant to decarbonization in South Italy: land-based wind and solar *vs.* exclusive solar rooftop, extra cost of a veto on nuclear, conservative assumptions on future storage technology and the role of pumped hydro storage, lack of low-cost geological storage of hydrogen and the industrial competitiveness of this carrier, and the methanation synergy with the agro-forestry sector. Our results quantify the high system cost of vetoes on land-based wind and solar. Nuclear may enter the optimal mix only with a veto against onshore wind and a hypothesis of equal project risk, hence an equal discount rate, with renewables. Scenarios with land-based wind and solar obtain low-cost hydrogen and thus allow industrial uses for this carrier. The methanation synergy with the agro-forestry sector does not offer a system cost advantage but improves the district's configuration. The extra cost of full decarbonization relative to unregulated fossil

*Istituto di Calcolo e Reti ad Alte Prestazioni, Consiglio Nazionale delle Ricerche, Via P. Bucci 41C, 87036 Rende (CS), Italy - luigi.moccia@icar.cnr.it

gas is small with land-based wind and solar, and very significant with vetoes to these technologies.

Keywords: energy system optimization; renewable-based scenarios; hydrogen; methanation; sustainable data centers

1 Introduction

Decarbonizing the energy system requires not only a steep increase in the electrification of end-use sectors such as transportation and heating, but also electro-fuels for some end-uses, and hence the need for a baseload supply of hydrogen, see e.g. Mathiesen et al. (2015); Connolly et al. (2016); Victoria et al. (2019). To this aim, we present an optimization model of a district supplying two baseload energy services with electricity and hydrogen as their carriers. We consider renewable and storage technologies with large techno-economic potentials in South Italy. The district is sized such that its services could be alternatively supplied by a nuclear reactor. By so doing, the model's results can offer a comparison for a given territory between the choice of a renewable *vs.* nuclear-based energy district. Nuclear energy is not currently part of the Italian energy supply, but in 2024 the government expressed a willingness to evaluate this technology for 2040 (MONTEL, 2024). This nuclear-sized baseload district has the further advantage of constituting an elementary building block for national scenarios. The purpose in this case would only be illustrative since several limitations are implied in a single-district model, as discussed in the following.

The baseload supply of energy services by renewables has been studied by Fasihi and Breyer (2020). The advantage of renewables with high capacity factors in global energy scenarios has been motivated by Afanasyeva et al. (2018) and Satymov et al. (2022) for wind and solar, respectively. Energy system optimization by open-source methods has been developed by several research groups, e.g. Schlachtberger et al. (2018); Lombardi et al. (2020); Tröndle et al. (2020); Neumann and Brown (2021). With respect to this literature stream, we want to address the following five points that are motivated by the specific context of South Italy but may be of general interest.

- *Photovoltaic* (PV) with high capacity factor as allowed by ground-based PV with mono-axial tracking *versus* solar rooftop.
- Prospective onshore wind with site-specific optimization.
- Conservative assumptions on short and medium-term storage technologies and the *Pumped Hydro Storage* (PHS) as a multi-benefit option.
- Lack of low-cost geological storage for hydrogen.
- Synergies with the agro-forestry sector.

It is well known that wind and solar complementarity reduces the supply cost of renewable-based energy systems (Takle and Shaw, 1979; Miglietta et al., 2017; Jurasz et al., 2020; Wohland et al., 2021; Breyer et al., 2022; Nyenah et al., 2022). This complementarity is particularly relevant for industrial plants requiring high capacity factors, as is the case for hydrogen and, in general, electro-fuel production (Blanco and Faaij, 2018). Moreover, the supply of baseload renewable electricity is a topic of increasing interest for sustainable data centers. This has sparked our interest in wind and solar hybrid districts where both sources are deployed with high capacity factors.

Ground-based Photovoltaic (GPV) is often underappreciated and dismissed for its hypothesized land impacts. Two well-established lines of reasoning question this criticism, and our analysis contributes to a third one. These three lines are briefly mentioned in the following, and the third is explored further in this paper. First, even with the massive deployment of GPV, the area required would not be so large that it would significantly interfere with other uses such as food production and natural habitat (Jacobson, 2020). Second, simple eco-design measures in GPV may yield net benefits for other socio-environmental objectives. The multi-criteria configuration of GPV traces back to the report of Macknick et al. (2013) and has been recognized as an example of green infrastructure (Semeraro et al., 2020). For instance, Semeraro et al. (2022a) highlight the potential of GPV for restoring wetlands, and the agricultural and ecosystem services of GPV as habitat for pollinator insects are discussed in Semeraro et al. (2018); Walston et al. (2018); Armstrong et al. (2021); Semeraro et al. (2022b). Third, there is a

systemic advantage to GPV with mono-axial tracking *versus* solar rooftop. Our results will show that by vetoing GPV, the energy system cost will increase not only due to the higher cost of solar rooftop per unit of energy *produced*, but also for the following reason. The lower capacity factor of solar rooftop *versus* GPV increases the cost of energy *delivered*, since it augments the required generation and storage capacities. This systemic view may integrate classical *Life-Cycle Assessment* (LCA) studies where photovoltaic plants are appraised per unit of energy produced. For example, Danelli and Brivio (2021), following the guidelines of Raugei et al. (2021), study several environmental impact categories for three types of PV plants (ground-based with tracking, rooftop, and agrivoltaic without tracking) in two locations (South and North Italy). Apart from the land use category, the environmental impacts are approximately inversely proportional to the PV plant's capacity factor. Given these results, we inquire about the energy system effects of vetoes on land-based wind and solar beyond the boundaries of LCA studies.

The techno-economic potential of onshore wind in Italy is underestimated by averaging wind speed over large areas. In an orographically complex country such as Italy, this wide-area averaging bias is significant (Pelser et al., 2024), and it is further compounded by assuming only one average wind turbine type and hub height instead of optimizing according to local conditions. Moreover, wind turbine technology and management have progressed in the last two decades (see e.g. Rinne et al. (2018) for Finland, and Lantz et al. (2019) for the US), and further near and medium-term improvements are expected (Wiser et al., 2021). Hence, prospective assumptions on wind technology should be considered for 2050 decarbonization scenarios instead of historical data, which in Europe are biased by the early deployment of this technology two decades ago. These considerations motivate our approach for using capacity factors as in Ryberg et al. (2019), where prospective wind turbines are granularly optimized.

For short and medium-term storage, we focus on PHS for two main reasons. First, PHS is a mature technology, and further cost decreases are not expected. As our results will show, the plausible trends in wind and solar technologies are sufficient to

obtain a low-cost supply of reliable energy services under this worst-case assumption on storage technologies, i.e. no breakthrough. Thus, a focus on PHS confutes that a renewable-based energy system lacks techno-economic feasibility for expensive storage. Second, closed-loop off-river PHS may synergize with other public interests besides decarbonization, namely minimizing extreme weather risks under climate change, such as droughts and floods. For this line of inquiry on so-called blue infrastructure in Italy, see Frigerio et al. (2012); Fanelli et al. (2018). Regarding PHS techno-economic potentials, Stocks et al. (2021) locate worldwide closed-loop off-river PHS plants by the methodology of Lu et al. (2018). Simon et al. (2023) validate the method and results of Stocks et al. for the US. For Italy, Stocks et al. individuate 2347 PHS sites with a storage capacity of 64 TWh. This value is two orders of magnitude larger than what is reasonably necessary in this country. Therefore, by including PHS as a storage option, we base our model on a mature and scalable technology with potential co-benefits.

We assess the long-term storage of electricity by hydrogen in surface tanks and synthetic methane in geological storage. This modeling choice is motivated in the following. Italy lacks salt caverns, the more favorable geological structures for underground hydrogen storage (Caglayan et al., 2020). We note that the Italian potential for underground hydrogen storage in less favorable geological structures is not zero (Barison et al., 2023), and this country could benefit from a European hydrogen infrastructure (Neumann et al., 2023). Both options could lower the storage cost of hydrogen, but we prefer to err on the cautious side and assume that hydrogen in Italy may only be stored in surface tanks. Conversely, the geological storage capacity of fossil gas in Italy is overabundant for plausible scenarios in which synthetic methane is deployed as seasonal and strategic storage. Synthetic methane is usually referred to as electro-methane, and in the following is indicated by e-CH₄. Methanation has the disadvantage of additional conversion losses for the hydrogen required as input. Moreover, it requires a source of non-fossil CO₂ that may be supplied by *Direct Air Capture* (DAC) with a corresponding increase in cost and primary energy. The significant advantage

of e-CH₄ is its suitability for the already built storage infrastructure for fossil gas. As shown in the following, the optimal long-term storage option for South Italy is e-CH₄ because of the lower cost for geological storage relative to surface tanks.

Methanation is increasingly appraised in the energy scenario literature by a synergy with the agro-forestry sector, which is relevant in South Italy. This synergy is usually referred to as *Power-And-Biomass-to-Gas* (P&B2G), see for example ADEME (2018); Shirizadeh and Quirion (2022); Shirizadeh et al. (2022); Shirizadeh and Quirion (2021) for France, Mortensen et al. (2020) for Denmark, Carbone et al. (2021); Pierro et al. (2021) for Italy, and Korberg et al. (2021) for the whole Europe. We follow this approach by considering optional CO₂ feedstock from a biogenic source. By so doing, we can study the competitiveness of biogenic CO₂ *versus* DAC as an input for the methanation process. We also include an optional source of biogenic methane to assess its competitiveness *versus* e-CH₄.

The model is implemented in the framework *Python for Power System Analysis* (PyPSA) (Hörsch et al., 2018). For transparency and replicability (Morrison, 2018), our code, data, and results are available at the Git-Hub repository Moccia (2024).

1.1 Outline

The remainder of this paper is structured as follows. Section 2 introduces our optimization model first qualitatively and then formally. The model is instantiated by techno-economic parameters sourced from the literature and reported in Section 3. Section 4 presents the main scenarios we use to answer our research questions, and Section 5 discusses their results. Section 6 draws some conclusions and indicates future work. Auxiliary scenarios and results are presented in Appendices A and B.

2 Model

The model is qualitatively described in Section 2.1, illustrated by a graph in Section 2.2, and presented as a linear program in Section 2.3. Major and minor limitations are

discussed in Section 2.4.

2.1 Qualitative description

The optimization model minimizes the system cost of the technologies activated in the energy district. The system cost is the sum of actualized capital expenditures, and operations and maintenance costs. The parameters of the technologies are estimated for the year 2050 and presented in Section 3. There are two demands for energy services, with electricity and hydrogen as their carriers. The electric and hydrogen demands are constant for each timestep in the studied time horizon, i.e. are of the baseload type (Appendix A removes the baseload assumption with a time-varying profile of electricity). The timestep is one hour, and the time horizon is a non-leap year of 8760 hours. The demands are set to 1 GW for the electricity and 0.25 GW for the hydrogen¹. The model has a parametric CO₂ budget for its emissions, but in the main scenarios studied in this paper, this budget is set to zero, a normative assumption for the year 2050. As shown in the following, when accounting for the electricity input of the electrolysis process, the total power required for this district based on nuclear would be similar to that offered by a new nuclear reactor, i.e. a generation III/III+ reactor. In this sense, we deal with a nuclear-sized baseload district, even though the minimum cost optimization favors renewable sources in South Italy. Similar districts can serve as elementary building blocks for national scenarios, albeit only for illustrative purposes, given the intrinsic limitations of single districts. For example, based on a first approximation assessment, if Italy requires 46 GW of baseload electricity and 11 GW of baseload hydrogen by 2050, 46 such districts would be needed.

The model considers the following four technologies as non-fossil primary energy sources:

- Onshore wind.
- GPV with mono-axial tracking, in the following also referred to as *solar utility*.

¹relative to the lower heating value of this fuel.

- Photovoltaic with a fixed orientation as it usually occurs with *solar rooftop*.
- Nuclear fission.

Solar rooftop is further differentiated in two alternative cases, in the sense that only one can be activated in a scenario according to a flag parameter. The two cases differ in the solar *Capacity Factors* (CFs) according to the following assumptions:

- Optimal fixed tilt and the same solar availability as for solar utility. These assumptions yield a relatively high capacity factor, and this case is indicated as *solar rooftop high CF*.
- Assumptions described in Section 3.3 aimed at a more realistic CF for solar rooftop. This case is indicated as *solar rooftop low CF*.

The model also includes a source of fossil gas, which is constrained to zero by the CO₂ emission limit. This limit can be relaxed to draw insights into the extra cost of full decarbonization, and this analysis is carried out in Appendix B. Note that fossil gas cost influences the shadow price of CO₂, i.e. the dual variable associated with the decarbonization constraint.

The performances of the considered renewable technologies depend on their localization, and our assumptions are reported in Section 3.3.

The direct storage of electricity is allowed by two technologies:

- Li-ion battery.
- Closed-loop off-river pumped hydro storage.

The storage lengths of these two technologies are variables to be optimized.

The indirect storage of electricity is allowed by hydrogen and synthetic methane by the following technologies:

- electrolysis;
- methanation;

- DAC of CO₂.

Both hydrogen and synthetic methane can operate as long-term storage. Methanation is modeled as a continuous process only partially modulable at 30% of the installed capacity. The maximum annual capacity factor of the electrolysis is set to 90%. The capture of CO₂ by DAC requires a heat pump as an auxiliary for the thermal input of this process. CO₂ storage in surface tanks is included to decouple electrolysis and methanation processes. System cost minimization determines the optimal capacities of these long-term storage options and their auxiliaries. The optimal mix between hydrogen and e-CH₄ is thus an optimized outcome and not an input parameter.

The model considers an optional CO₂ feedstock flow from a biogenic source (bio-CO₂). When bio-CO₂ is competitive, it fully or partially replaces CO₂ from DAC. In this case, the produced methane should be referred to as e-bio-CH₄, but we maintain the label e-CH₄ for simplicity. We also include an optional source of biogenic methane (bio-CH₄) to assess its competitiveness *versus* e-CH₄.

Because of these modeling choices, we have three possible sources of methane that can be used as an auxiliary carrier inside the energy district: two sources are renewable, e-CH₄ and bio-CH₄, and one is fossil. Methane can be used to generate electricity by an *Open Cycle Gas Turbine* (OCGT). Hydrogen, in addition to being supplied as final demand, can be used to generate electricity by a *Fuel Cell* (FC).

2.2 Graph representation

Fig. 1 illustrates the connections between the sub-systems of the model by a directed graph. The two demand nodes, for electricity and hydrogen, are represented as trapezoids, and their inputs derive from bus nodes depicted as rectangles. A bus node represents an energy/feedstock carrier and its input-output equilibrium constraint for each timestep of the time horizon. The inputs of the electricity bus derive from generator nodes depicted as circles. Generator nodes produce electricity according to constraints specific to the technology. For example, the nuclear node generates electricity with a constraint on the maximum annual capacity factor of 90%; the wind node gen-

erates electricity according to the assigned hourly availabilities. Generator nodes of primary sources do not have upstream dependencies. Conversely, generator nodes of storage technologies have specific upstream dependencies. For example, the generator node PHS depends on the state of charge of its upper basin; the OCGT node requires a methane input derived from the bus for this fuel. As explained below, arcs to bus, storage, and auxiliary nodes illustrate these dependencies. Storage nodes are depicted as cylinders; at these nodes, the hourly equilibrium considers their state of charge. Storage nodes of primary sources for fuel and feedstock do not have an input, and their state of charge can be depleted during the time horizon starting from a given initial level. Storage nodes of auxiliary technologies have both input and output, and their state of charge is a variable constrained to equal values at the beginning and end of the time horizon. The auxiliary nodes, depicted as squares, represent processes such as methanation, electrolysis, hydrogen compression, DAC, thermal production by heat pump, and battery and PHS loading phases. The auxiliary nodes represent loads the four buses serve for electricity, hydrogen, methane, and CO₂. As will be detailed in Section 4, the model allows to exclude some pathways in this graph to assess the impact of exogenous technological choices on the optimal system cost, such as a veto on ground-based PV, or onshore wind, or nuclear, or any suitable combination of vetoes. Flag parameters, i.e., binary values, make specific energy pathways available or not in the model-building phase.

2.3 Linear program

Let \mathcal{N} and \mathcal{A} be the set of nodes and arcs for the graph of Fig. 1, respectively. For a node n , the set $\delta(n)^+$ indicates the outgoing arcs, and the set $\delta(n)^-$ the incoming ones. For simplicity, when these sets have cardinality one, the outgoing and incoming arcs are $a(n)^+$ and $a(n)^-$, respectively. Let $\mathcal{T} = \{0, \dots, 8759\}$ be the set of hourly timesteps in one year. The subset of nodes corresponding to power, auxiliary, and storage technologies that, when activated, require a capital expenditure is \mathcal{N}_c . A non-negative continuous variable y_n is associated with node $n \in \mathcal{N}_c$, and expresses the installed capacity, if

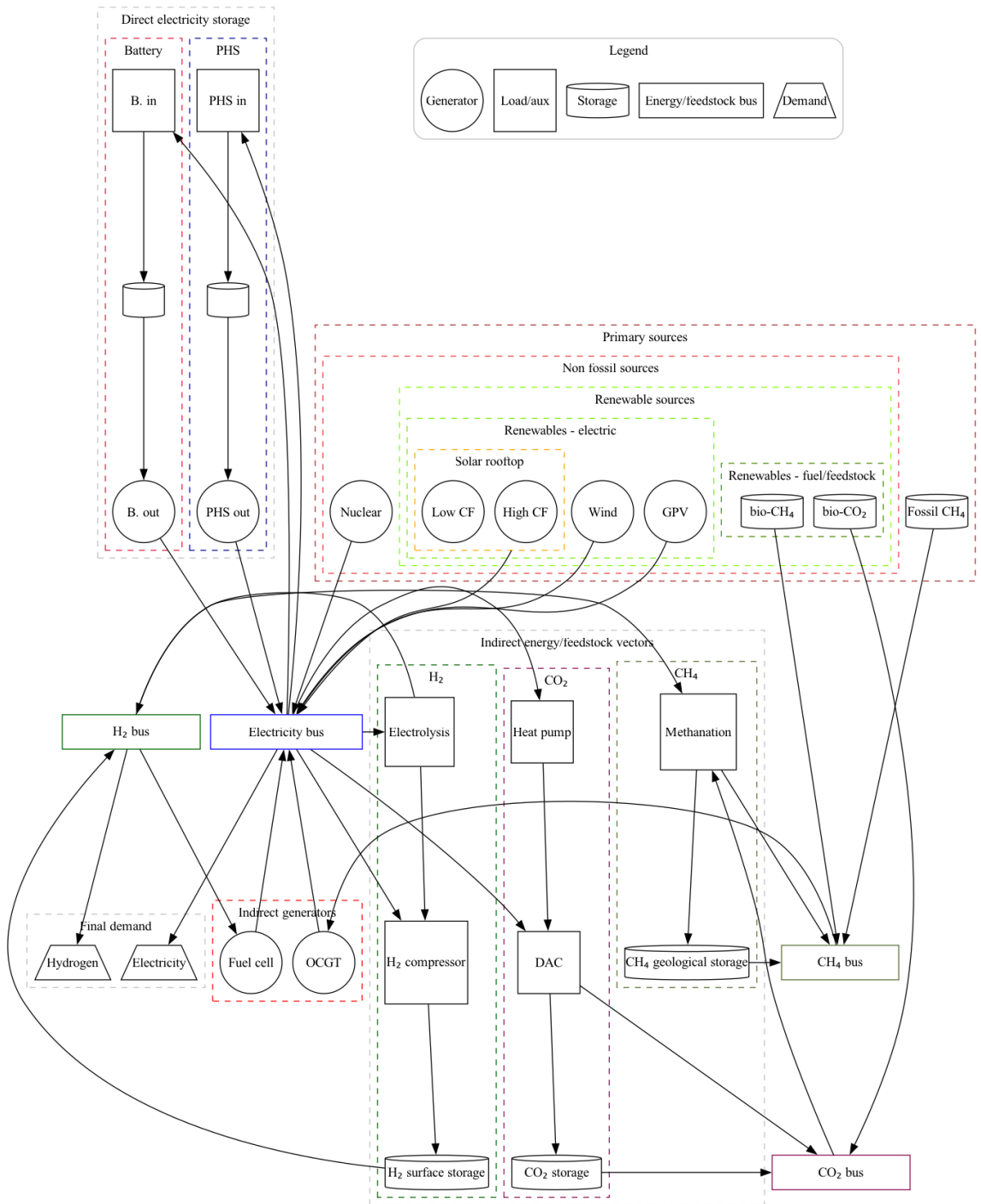


Figure 1: Graph of the model's components and their relationships.

any. The unitary fixed cost of this capacity is c_n , the sum of the annuity, and fixed operations and management costs. We distinguish the following subset of nodes to enforce technology-specific constraints. The subset \mathcal{N}_p corresponds to technologies, e.g. nuclear, that can operate up to the maximum installed capacity with an annual constraint on the capacity factor $u_n, n \in \mathcal{N}_p$ with $u_n \leq 1$. The subset \mathcal{N}_a groups auxiliary technologies where a constraint on the maximum installed capacity is enforced. The subset $\mathcal{N}_{a,l} \subset \mathcal{N}_a$ represents auxiliary technologies, methanation in our model, where the hourly capacity factor, if the technology is activated, must have a lower bound w_n with $w_n \leq 1$. The subset \mathcal{N}_v refers to wind and solar, which at each timestep t are constrained by the availability factor $v_{n,t}, n \in \mathcal{N}_v, t \in \mathcal{T}$ with $v_{n,t} \leq 1$. A pair of nodes (n, m) in the set $\mathcal{P} \subset \mathcal{N} \times \mathcal{N}$ corresponds to technologies that require equal capacities at the charge and discharge nodes, as is the case for battery and PHS.

Non-negative continuous variables of energy and feedstock flows are $x_{a,t}$, with $a \in \mathcal{A}$ and $t \in \mathcal{T}$. A subset $\mathcal{A}_o \subset \mathcal{A}$ represents the arcs where variable costs occur with positive flows. The unitary variable cost of an arc is $o_a, a \in \mathcal{A}_o$ and expresses fuel or feedstock or operations and management costs.

The following subsets of nodes are used to enforce hourly balances. The subset \mathcal{N}_u indicates the nodes where the hourly input-output balance must consider an input transformation with a loss, the process efficiency being $\eta_a, a \in \delta(n)^-, n \in \mathcal{N}_u$. If the incoming arcs are more than one, they refer to different energy carriers or feedstock. For example, methanation requires hydrogen and CO₂. In these cases, the hourly balance must be enforced separately for every input. The subset \mathcal{N}_b corresponds to bus nodes where the hourly input-output balance is lossless. The subset \mathcal{N}_d indicates the final demand nodes where the incoming arc must be equal to the hourly demand $d_{n,t}, n \in \mathcal{N}_d$. The subset $\mathcal{N}_{a,s} \subset \mathcal{N}_a$ groups the nodes of auxiliary technologies where the hourly balance is lossless. Input and output nodes of battery and PHS belong to this set since the charging and discharging losses are accounted for at the intermediate storage node as explained in the following. The subset \mathcal{N}_s refers to storage technologies and non-negative continuous variables $q_{n,t}$ express the hourly state of charge. The state

of charge, constrained by the maximum installed capacity, is defined by flow conservation with charging and discharging losses $\eta_a, a \in \delta(n)^- \cup \delta(n)^+, n \in \mathcal{N}_s$, and satisfies additional constraints depending if the storage capacity is cyclical or depletable. The timestep that precedes t is $\tau(t)$ with $\tau(t) = t - 1$ if $t > 0$ and $\tau(t) = |\mathcal{T}| - 1$ if $t = 0$. Let $\mathcal{N}_{s,c}$ be the subset of storage technologies that are cyclical, and $\mathcal{N}_s \setminus \mathcal{N}_{s,c}$ refers to those depletable. The cyclical storage is such that the first and last timesteps have equal states of charge. The depletable storage starts with a given level of charge $\hat{q}_n, n \in N \setminus \mathcal{N}_{s,c}$. The arc a_f indicates fossil gas entering the energy district. Given a unitary emission factor e of fossil gas, an annual emission budget \hat{e} is applied.

The linear program is:

$$\text{minimize} \sum_{n \in \mathcal{N}_c} c_n y_n + \sum_{a \in \mathcal{A}_o} \sum_{t \in \mathcal{T}} o_a x_{a,t}, \quad (1)$$

subject to

$$\sum_{a \in \delta(n)^+} x_{a,t} \leq y_n, \quad \forall n \in \mathcal{N}_p \cup \mathcal{N}_a, t \in \mathcal{T}, \quad (2)$$

$$x_{a(n)^+, t} \leq v_{n,t} y_n, \quad \forall n \in \mathcal{N}_v, t \in \mathcal{T}, \quad (3)$$

$$w_n y_n \leq \sum_{a \in \delta(n)^+} x_{a,t} \quad \forall n \in \mathcal{N}_{a,l}, t \in \mathcal{T}, \quad (4)$$

$$\sum_{a \in \delta(n)^+} \sum_{t \in \mathcal{T}} x_{a,t} \leq |T| u_n y_n \quad \forall n \in \mathcal{N}_p, \quad (5)$$

$$y_n = y_m \quad \forall (n, m) \in \mathcal{P}, \quad (6)$$

$$\sum_{a \in \delta(n)^+} x_{a,t} - \eta_h x_{h,t} = 0 \quad \forall n \in \mathcal{N}_u, h \in \delta(n)^-, t \in \mathcal{T}, \quad (7)$$

$$\sum_{a \in \delta(n)^+} x_{a,t} - \sum_{a \in \delta(n)^-} x_{a,t} = 0 \quad \forall n \in \mathcal{N}_b \cup \mathcal{N}_{a,s}, t \in \mathcal{T}, \quad (8)$$

$$x_{a(n)^-, t} = d_{n,t} \quad \forall n \in \mathcal{N}_d, \quad (9)$$

$$q_{n,\tau(t)} + \sum_{a \in \delta(n)^-} \eta_a x_{a,t} - \sum_{a \in \delta(n)^+} \eta_a^{-1} x_{a,t} = q_{n,t} \quad \forall n \in \mathcal{N}_s, t \in \mathcal{T}, \quad (10)$$

$$q_{n,t} \leq y_n \quad \forall n \in \mathcal{N}_s, t \in \mathcal{T}, \quad (11)$$

$$q_{n,t=0} = q_{n,t=|\mathcal{T}|-1} \quad \forall n \in \mathcal{N}_{s,c}, \quad (12)$$

$$q_{n,t=0} = \hat{q}_n \quad \forall n \in \mathcal{N}_s \setminus \mathcal{N}_{s,c}, \quad (13)$$

$$\sum_{t \in \mathcal{T}} e x_{a_f, t} \leq \hat{e} \quad (14)$$

$$y_n \geq 0 \quad \forall n \in N, \quad (15)$$

$$x_{a,t} \geq 0 \quad \forall a \in \mathcal{A}, t \in \mathcal{T}, \quad (16)$$

$$q_{n,t} \geq 0 \quad \forall n \in \mathcal{N}_s, t \in \mathcal{T}. \quad (17)$$

The objective function (1) minimizes the system cost, sum of annuities, and fixed and variable costs, including fuel and feedstock costs. The installed capacities are enforced by constraints (2) for dispatchable and auxiliary technologies. Constraints (3) ensure that the hourly output of variable renewables is not larger than the installed capacity diminished by the availability factor. The lower modulation limit for methanation is described by constraints (4). The annual maximum capacity factor for technologies such as nuclear is defined by constraints (5). Equal charging and discharging

capacities of some storage technologies are ensured by constraints (6). Constraints (7) define the hourly balances of nodes where the inputs are transformed with an efficiency loss. Constraints (8) refer to lossless hourly balances at bus and auxiliary nodes. The final demands are satisfied by constraints (9). The hourly state of charge variables are defined by constraints (10) accounting for charging and discharging losses, if any. The maximum state of charge must be no larger than the installed capacity by constraints (11). Constraints for cyclical and depletable storage technologies are enforced by constraints (12) and (13), respectively. Constraint (14) is the CO₂ emission limit. The domains of the variables are in (15) — (17).

Dual variables represent shadow prices. For example, the dual variable associated with constraint (14) is the shadow price of CO₂. The shadow prices allow us to compute cost-revenue balances for all the district's sub-systems.

The linear program is coded in PyPSA and executed by a commercial solver (Gurobi version 10.0). The number of variables and constraints are $\sim 4 \times 10^5$ and $\sim 8 \times 10^5$, respectively. The average execution time is approximately one minute on a desktop computer.

2.4 Limitations

A single-district energy system reliant on time-varying sources such as wind and solar has its main limitation in the absence of geographical area diversification, which requires electricity transmission. With the hypothesis of no transmission between areas with different temporal availabilities of wind and sun, the studied energy system must be regarded as a worst-case. It is, in fact, well known that renewable-based scenarios over wider geographical areas yield lower system costs thanks to the increasing negative correlation between wind and solar availabilities, see e.g. Schlachtberger et al. (2017) for the cost-optimal expansion of transmission in a European-wide renewable-based electricity sector.

A fixed demand is another worst-case assumption. Demand flexibility decreases system cost in renewable-based energy systems. This option may considerably in-

crease in the near future with battery-electric vehicles, heat pumps, and inexpensive non-electric storage on the end-use side such as thermal storage. For the opportunities of massive thermal energy storage see Lund et al. (2016, 2021); Paardekooper et al. (2022), and for synergies between the electricity sector and thermal end-uses see Möller et al. (2019); Jacobson et al. (2022); Thellufsen et al. (2023). These end-use options can be studied as well in a single-district setting but are better assessed at least at a regional or national scale and are out of the scope of this paper. We remark that by focusing on baseload electricity our results are not largely affected by this worst-case assumption. A baseload demand will always, by definition, be present in future energy systems, even with higher flexibility.

In this paper, we have not considered technologies that could reduce the system cost further. For example, we did not include the *Adiabatic Compressed Air Energy Storage* (A-CAES), which could replace PHS at a slightly lower system cost. According to Aghahosseini and Breyer (2018), A-CAES techno-economic potential in Italy is vast; therefore, this option merits further assessment. Our rationale for excluding A-CAES is the larger uncertainty of its future cost compared to a mature technology such as PHS. This choice aligns with our focus on conservative assumptions about 2050 decarbonization technologies.

For simplicity, some model refinements were not included in the main scenarios presented in this paper, but they can yield plausible, albeit low, system cost reductions. Examples of these minor refinements are:

- Combined cycle gas turbine (this technology is activated for the scenarios presented in Appendix A).
- Multi-fuel turbines, e.g. gas turbines that can use both methane and hydrogen.
- Sub-networks in direct current to improve the relationships between some sources and electrochemical storage technologies.
- Thermal sub-networks to improve synergies between endo and exo-thermal processes.

3 Data

The default techno-economic parameters in the PyPSA framework are mainly derived from the *Danish Energy Agency* (DEA) reports (DEA, 2022a,b,c). DEA is an institution that has historically led the transition from fossil to renewable energy. We have, therefore, decided to keep most of the default PyPSA assumptions with the following modifications.

We have chosen PHS as representative technology for medium-term storage for the reasons discussed in Section 1. PHS is a technology insufficiently detailed in DEA datasets, as expected, for its very limited potential in a country with flat orography such as Denmark. The choice of the surface tank for hydrogen storage induces as well an integration relative to standard PyPSA assumptions. Data selection for short, medium, and long-term storage is discussed in Section 3.1.

Another technology insufficiently described in the DEA reports is nuclear. For nuclear, we have used data from the *International Energy Agency* (IEA) report of Bouckaert et al. (2021) and Lazard (2019), as detailed in Section 3.2.

We diverge from standard PyPSA data assumptions also on the hourly availabilities of wind and solar. PyPSA generates these availability profiles by the code Atlite (Hofmann et al., 2021). We must meet the following conditions to tackle our research questions on the system advantages of ground-based solar and prospective onshore wind. For solar, we need to differentiate between the availability profiles of state-of-the-art PV plant with mono-axial tracking and a rooftop installation. For wind, we want to avoid the underestimation of its potential caused by three main factors:

- Wide-area integration in an orographically complex country such as Italy.
- Generic wind turbine power curve instead of one optimized for specific local conditions.
- Assessment limited by current technology instead of that forecasted for the year 2050.

To this aim, we use the open dataset Renewables.ninja² (Pfenninger and Staffell, 2016; Staffell and Pfenninger, 2016) oriented for wind by the results of Ryberg et al. (2019) as described in Section 3.3.

The techno-economic parameters are synthesized in Tab. 1 with their literature sources. The exogenous bio-CH₄ and bio-CO₂ cost parameters are 40 €/MWh_{th} and 70 €/ton, respectively. Fossil gas is assumed to be 20 €/MWh_{th}. All monetary values refer to the year 2015 or years before 2022 when inflation significantly increased cost assessments.

The annuity of an investment I with an expected lifetime of n years and a discount rate r is computed as

$$I \frac{r}{1 - \frac{1}{(1+r)^n}}. \quad (18)$$

We highlight that the discount rate is the parameter with the largest impact on the results. Section 4 details how we deal with this parameter's sensitivity.

3.1 Parameters for storage

We have derived the PHS techno-economic parameters from Guerra et al. (2021), a recent paper with a focus on future storage technologies. We can benchmark the PHS assumptions of Guerra et al. with the most recent large project in South Italy. A PHS plant of 1 GW power and 6 GWh storage capacity was completed in Presenzano (Caserta) in 1990. At its current value, the investment of the Presenzano plant can be estimated at approximately one billion euros. With the parameters of Tab. 1, such a plant would require an investment of 1.3 bln €. Given this, we consider using Guerra et al. for PHS in Italy sufficiently conservative. To maintain coherence among storage technologies that can have overlapping system roles, we have decided to use the Guerra et al. parameters as well for battery storage (in their paper indicated as “short term storage”).

Industrial-scale storage in surface tanks is extensively reported in IEA (2019), the

²<https://www.renewables.ninja/>

source we have also used for the electrolysis cost parameter.

3.2 Parameters for nuclear

The International Energy Agency estimates for the year 2050 in the European Union that a nuclear reactor will have an overnight capital cost of 4500 \$/kW, an operation and management cost (OPEX) of 35 \$/MWh, a financing rate of 8%, with a resulting *Levelized Cost of Electricity* (LCOE) of 115 \$/MWh when the annual capacity factor is 70% (Bouckaert et al., 2021). This cost disaggregation needs to be improved for our model since the capacity factor itself is an outcome of the system cost minimization. Therefore, we need to differentiate the nuclear OPEX between the fixed cost components that are independent from the capacity factor (FO&M) and those that are proportional to the produced electricity (VO&M). To this purpose, we use data from the report Lazard (2019) that offers this disaggregation. The nuclear investment cost is computed as follows. Let C be the overnight capital cost, n the number of years for the building phase, and r the financing rate. We conservatively³ assume a linear capital expenditure during the building phase. Then the investment cost I , usually referred to as CAPEX, is:

$$I(C, n, r) = C \times \left(1 + \sum_{i=1}^n \frac{(1+r)^{n+1-i} - 1}{n} \right) \quad (19)$$

A building phase of 7 years and the other parameters listed above yield an investment cost of 6195 €/kW. A unitary exchange rate between the euro and the US dollar has been assumed for all these CAPEX and OPEX values. Under these hypotheses, the nuclear OPEX is 27.7 €/MWh when the CF is at its maximum value of 90%, and is 32.1 €/MWh when the CF is 70%. The resulting nuclear LCOE with maximum CF is 91.1 €/MWh, and is 113.6 €/MWh with a CF of 70%. Thus, the chosen parameters are coherent with Bouckaert et al. (2021). Moreover, as discussed in Section 5.2, our results show that in 2050, with low-cost solar, the nuclear CF can be ~70%. Whether

³According to Shirizadeh and Quirion (2022) a linear capital expenditure during construction induces an underestimation of the financing cost for nuclear.

the LCOE of this technology will be economically sustainable under these conditions is debatable.

The above assumptions are relatively favorable to nuclear in our single-district comparison with variable renewables. We are assuming a maximum capacity factor of 90% for nuclear, expressed as a constraint on the annual output. This hypothesis is not realistic for a single reactor since it implicitly requires a national grid on which several reactors optimally schedule their maintenance and refueling throughout the year. For a single reactor, as it would be in the case of the single district, nuclear unavailability would not be optimally distributed during the year but concentrated in a given period, for example, one month in summer. This unavailability would be costlier to manage relative to the constraint on the maximum annual capacity factor that we have chosen. Our model implements a variant where the nuclear unavailability is concentrated instead of constrained by the annual capacity factor. As expected, nuclear competitiveness worsens in this model variant. These results are omitted in this paper but are available in the online code repository Moccia (2024).

Another simplification that favors nuclear relative to renewables is the assumption of a fixed lifetime for the electrolyser. In Tab. 1, the cost parameters for the electrolysis are derived assuming an annual capacity factor of 57%. Therefore, the resulting electrolysis lifetime of 20 years is a cost underestimation for a nuclear-based district where the hydrogen process CF would be at its maximum value of 90%. We comment further on this issue in Section 5.5.

3.3 Hourly availability profiles of wind and solar

Ryberg et al. (2018, 2020) study the available areas for onshore wind in Europe according to a comprehensive set of exclusion criteria. For these available areas, Ryberg et al. (2019) define a localization procedure for individual wind turbines and an optimization method for turbine sizing under prospective technology estimated for the year 2050. The prospective technology is derived from the current Vestas 4.2-136 model, but the specific power and hub height are determined such that the multi-year LCOE

is minimized for each turbine location. These results are relevant for our study since they offer a geographical distribution of wind potential under realistic 2050 technology assumptions. For Italy, the results of Ryberg et al. (2019) are as follows. The total techno-economic potential is ~600 GW with a CF of 25%, i.e. a generation potential of 1300 TWh/y, and a subset of 153 GW yields a CF of 33%. The subset with LCOE not larger than 56 €/MWh has a cumulated capacity of 100 GW with CFs in the 31—51% range and an average value of 35%. Fig. 2 illustrates the average and marginal CFs of the cumulated capacity ordered with increasing LCOE. Fig.3 depicts the geographical distribution of the 100 GW subset with the lowest LCOE aggregated at the provincial level (level 3 of the *Nomenclature of Territorial Units for Statistics* (NUTS)). Fig. 4 illustrates the geographical distribution of this subset with points color-coded by the CF for each turbine. Four-fifths of this potential is located in South Italy, where the best national solar resource is also available. Conservatively, we locate the energy district in Cosenza province, Calabria region. This area does not offer the highest capacity factors for wind and solar in South Italy, these being Sicily for solar and Sardinia for wind. We have extracted from the online service Renewables.ninja a wind turbine availability curve located in Cosenza province for the year 2010. According to a study by the Italian electric grid operator, the meteorological year 2010 is representative of the long-term average for wind and solar in this country (TERNA-SNAM, 2022). The selected wind turbine is a Vestas 4000-150 with a hub height of 80 meters and a CF of 33%. Thus, we use a CF value representative of 153 GW for onshore wind in Italy, according to Ryberg et al. (2019). We also extracted two PV availability profiles for the same year and location from the online service Renewables.ninja. One for the photovoltaic plant with mono-axial tracking, yielding a CF of 22.7%, and the other for the rooftop photovoltaic with optimal tilt, with a CF of 17.7%. This last curve may be regarded as a best case for PV rooftop performances and may not be representative of the average rooftop installations, not even in South Italy. In fact, rooftop installations are typically constrained by orientation, shading, and more cumbersome maintenance. Current PV installations in Italy are mostly rooftop, and the average CF in 2021 has been ~13% (GSE, 2022).

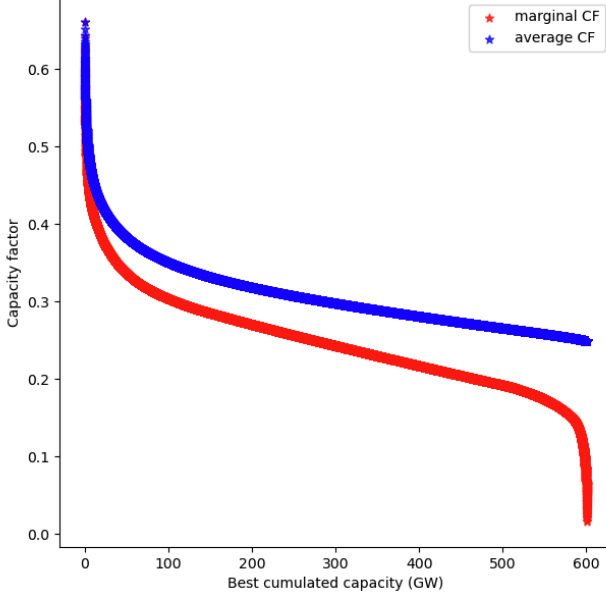


Figure 2: Onshore wind potential in Italy, average and marginal capacity factors of the cumulated capacity with increasing LCOE. Our elaboration from data of Ryberg et al. (2019).

To assess more realistic scenarios where there is a veto on ground-based PV, we have selected from the online service Renewables.ninja a solar availability curve with a CF of 13.9% by locating this plant in North Italy, province of Mantova. This curve might be regarded as more representative of the scenarios with a veto on ground-based PV. These four hourly availability profiles are illustrated in Fig. 5.

4 Scenarios

We first present the two main sets of scenarios for our model. Section 4.1 introduces a scenario set where the discount rate is constant among technologies, and Section 4.2 defines a second set with technology-specific discount rates. The scenarios in these two sets exclude biogenic gases, and this constraint is relaxed in a scenario presented in Section 4.3, along with scenarios to assess storage technologies. Two additional scenario sets are reported in Appendices A and B.

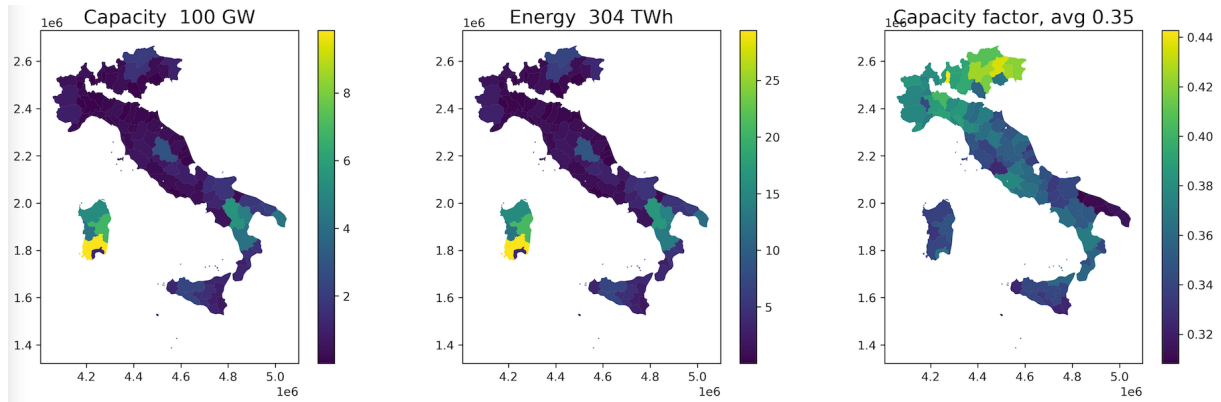


Figure 3: Onshore wind potential in Italy, geographical distribution: the lowest LCOE 100 GW of potential (left), the corresponding distributions of annual production (center), and the average capacity factors (right). Our elaboration from data of Ryberg et al. (2019).

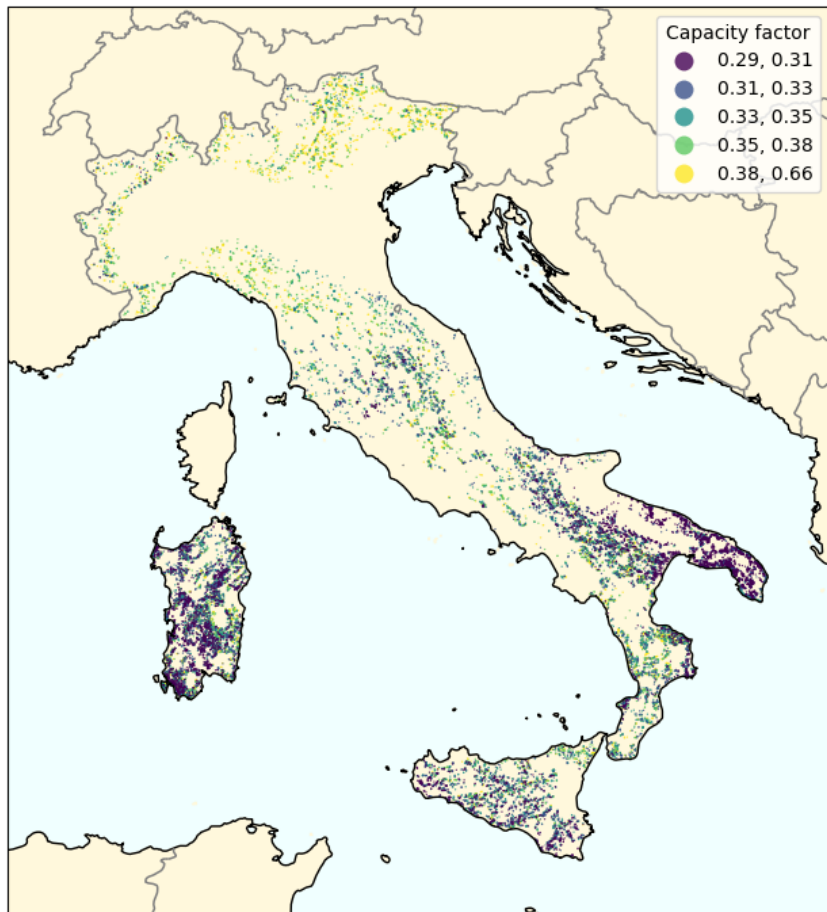


Figure 4: Onshore wind potential in Italy, geographical distribution of the lowest 100 GW potential: every point is a turbine, the color codes the CF range as in the legend. Our elaboration from data of Ryberg et al. (2019).

Table 1: Techno-economic parameters, sources and technical notes⁰

Technology	FO&M % I/y	VO&M €/MWh	Efficiency/other	Investment (I) €/MW or MWh	Lifetime y	Source
Onshore wind	1.18	1.22	-	963070	30	DEA (2022c)
Solar utility, with tracker	2.57	0.01 ¹	-	280000	40	DEA (2022c)
Solar rooftop, commercial	1.81	0.01 ¹	-	374880	40	DEA (2022c)
Nuclear	1.95 ²	12.4 ³	-	6195000 ⁴	60	Bouckaert et al. (2021); Lazard (2019)
Combined cycle gas turbine	3.25	4.0 ⁵	0.60	800000	25	DEA (2022c)
Open cycle gas turbine	1.8	4.5 ⁵	0.43	411840	25	DEA (2022c)
Li-ion battery, energy	-	-	-	115700	13	Guerra et al. (2021)
Li-ion battery, power	10.5	3.1	0.86	97800	13	Guerra et al. (2021)
Pumped hydro storage, energy	-	-	-	53100	55	Guerra et al. (2021)
Pumped hydro storage, power	0.77	1.0	0.782	1063320	55	Guerra et al. (2021)
Hydrogen storage, surface tank	4.0	-	-	2700	30	IEA (2019) ⁶
Electrolysis	1.5	-	0.74	450000	20	IEA (2019) ⁷
Hydrogen storage, compressor	4.0	-	0.05 ⁸	5903 ⁹	15	Stöckl et al. (2021)
Fuel cell	5.0	-	0.5	800000	10	DEA (2022c)
Methanation	3.0	-	0.78 ¹⁰	480580 ¹¹	20	Agora Energiewende (2018)
Heat pump ¹²	0.1	3.12	2.85 ¹³	700000	20	DEA (2022b)
CO ₂ storage tank	1.0	-	-	2528 ¹⁴	25	Lauri et al. (2014)
Direct air capture	4.95	-	(heat: 1.5, el.: 0.28) ¹⁵	4000000 ¹⁶	20	DEA (2022a)

⁰ In this table, all energy values of a fuel are referred to as the lower heating value (LHV).¹ PyPSA assumption: a negligible marginal cost to avoid wasting solar energy in storage cycling.² Derived from Lazard (2019) with USD-EUR parity, average cost case of 121 \$/kW-y and scaled to the CAPEX of note ⁴.³ It includes fissile material, low-cost case of Lazard (2019).⁴ Derived by formula 19 with overnight capital cost estimate of Bouckaert et al. (2021), 4500 €/kW, interest rate 8%, and 7 years construction time.⁵ It does not include fuel cost; in this model the gas turbines are multi-fuel and fuel costs are accounted separately either from primary sources such as fossil or bio-methane, or secondary sources such as electro-methane.⁶ Pag. 7 case "export terminal" and USD-EUR parity.⁷ Pag. 3 column "Long Term", USD-EUR parity; for the 20y lifetime the underlying assumption is a stack lifetime of 10⁵ hours and 5000/y of full load equivalent hours per year.⁸ Electricity input for compression in MWh_{el}/MWh_{H₂}.⁹ Investment per MW_{H₂} from the example in Table SI.4 of Stöckl et al. (2021), a CAPEX of 40,528 € for a compressed flow of 206 kg_{H₂} /h.¹⁰ Methanation efficiency relative to hydrogen, MWh_{CH₄}/MWh_{H₂}.¹¹ €/MW_{CH₄}.¹² Industrial heat pump, medium temperature up to 125 °C.¹³ Coefficient of performance (COP), i.e. MWh_{th}/MWh_e.¹⁴ €/tCO₂.¹⁵ Heat efficiency 1.5 MWh/tCO₂, electricity efficiency 0.28 MWh/tCO₂.¹⁶ €/tCO₂.

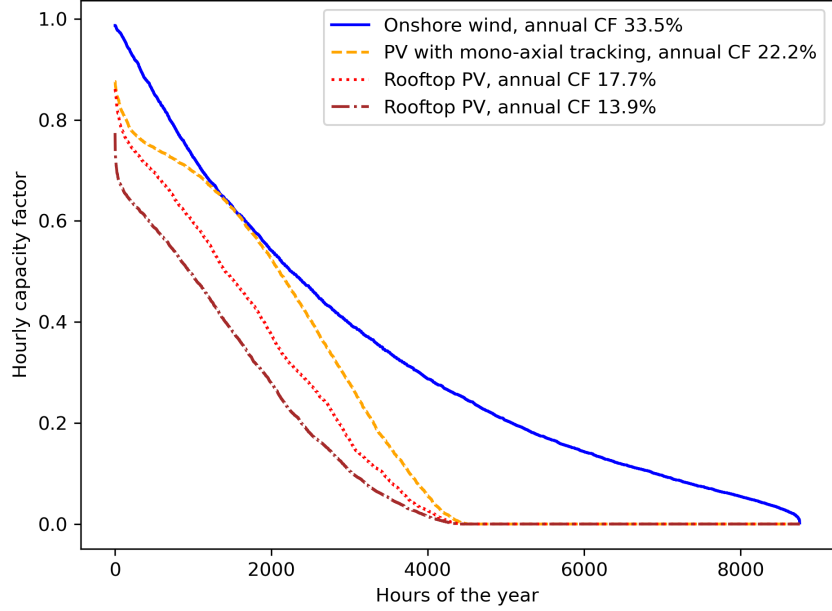


Figure 5: Duration curves of the hourly capacity factors for the four wind and solar technologies considered in the model.

4.1 Scenarios with a technology-agnostic discount rate

We define eight scenarios indicated by A—H where the discount rate is equal for all the technologies and set to 8%. In these scenarios, we exclude bio-gases for reasons discussed in Section 4.3 where this constraint is relaxed. In scenario A, besides the constraint on biogenic gases, all technologies are allowed, i.e. there are no vetoes. As will be detailed in Section 5, solving scenario A yields the dominance of GPV and onshore wind, and the following technologies are not activated for lack of competitiveness:

- solar rooftop;
- nuclear;
- fuel cell.

One of our research questions is the system advantage of GPV *versus* solar rooftop. To assess this advantage, we need to force the model to select solar rooftop. This is done in scenarios B and C, where GPV is constrained to zero, and solar rooftop is allowed with high and low capacity factors, respectively. As motivated in Section 3, solar rooftop with high capacity factor refers to a best-case for this technology, unlikely

to be representative of PV performances under a veto on GPV. Scenario C, solar rooftop with low capacity factor, is thus a more realistic scenario under a GPV veto. We remark that our hypotheses on solar rooftop with low capacity factor still include an optimistic bias, since we maintain the same PV cost parameter between the high and low capacity factor cases. We use this assumption to focus on the system's effects.

Scenario D is derived from scenario A by vetoing onshore wind. As expected, in scenario D, the dominant supply technology becomes GPV again. Therefore, to assess GPV *vs.* solar rooftop under a veto on onshore wind, we define two additional scenarios, E and F. In scenarios E and F, both onshore wind and GPV are constrained to zero, and solar rooftop is allowed similarly to scenarios B and C. In scenario G, all renewable sources are vetoed, and thus, the full decarbonization constraint leads to a 100% nuclear supply. In scenario H, we constrain to zero onshore wind, GPV, and nuclear. Solar rooftop is allowed with low CF. This scenario assesses an extreme lack of social license for both nuclear and renewable technologies.

4.2 Scenarios with a technology-specific discount rate

The scenarios introduced above implicitly include a favorable assumption toward nuclear. Namely, the project risk among technologies is the same, thus the technology-agnostic discount rate. The IEA report Bouckaert et al. (2021) differentiates between low project risk technologies such as onshore wind and GPV, and nuclear. This difference is relevant and realistic because of the widely recognized differences in project risk of these technologies, see e.g. Flyvbjerg (2017). We have included this enhanced realism in scenarios \dot{A} — \dot{H} : they inherit all the characteristics of the previously defined scenarios A—H but differ on the discount rate assumptions. Namely, nuclear faces a discount rate of 8%, and all other technologies are assessed by a discount rate of 3.2%, as in Bouckaert et al. (2021).

4.3 Scenarios to assess auxiliaries

In the scenarios presented above, the supply of biogenic gases is constrained to zero. This choice derives from the fact that scenario results vary widely on the amount of backup by OCGT. As detailed in the following section, scenarios where land-based wind and solar are vetoed do require a significant amount of long-term storage by synthetic methane. Allowing biogenic gases in these scenarios would yield a relevant role for these sources. These scenarios would be unlikely since vetoes to technologies with low or near-zero land impact, such as GPV and onshore wind, would naturally extend to more land-intensive bioenergies. Biogenic gases derived from agro-forestry residues and compatible with other socio-environmental and economic constraints would have a limited potential for the baseload supply of electricity and hydrogen, which is the focus of our model (see the discussion of the literature on the limits of human appropriation of biomass in Mortensen et al. (2020)). Given this, we explore the possible role of biogenic gases by a variant of the renewable scenario that is most parsimonious in terms of OCGT backup, which is scenario \dot{A} . We thus define scenario \dot{A}_b that inherits all characteristics of scenario \dot{A} but relaxes the zero availability constraint on biogenic gases.

We further explore variations of scenario \dot{A} by introducing the following scenarios with vetoes to storage technologies. In scenario \dot{A}_p we constrain to zero PHS, in scenario \dot{A}_m we veto methanation, and in scenario $\dot{A}_{p,m}$ we make unavailable both technologies.

5 Results

Figures illustrate the main results of a scenario, and the templates of these figures are presented in Section 5.1. Results of scenarios with technology-agnostic discount rates are discussed in Section 5.2, while Section 5.3 presents those with technology-specific ones. Section 5.4 comments on biogenic gases, PHS, and methanation system effects. A synthesis of the extra costs of the main vetoes is also provided here. Section 5.5

discusses the competitiveness of hydrogen for industrial uses, and Section 5.6 deals with the implications of our results for the geological storage capacity of synthetic methane in Italy.

5.1 Templates of the main figures

Four figures illustrate the main results of a scenario. The structure and interpretation of these figures are presented in the following using examples from scenario A, Figs. 6–9. As advised by Cramer et al. (2020), we use a linear color map for technologies with the aim of reducing reading difficulties for color-impaired persons.

Fig. 6 illustrates the main performance indices of the minimum system cost solution. The three bars report the percentage contribution of the technologies to the following system values, from top to bottom: primary generation, delivered electricity, and unitary cost of the delivered services. These three system values are listed as labels on the left vertical axis. The unitary cost index, indicated as *Levelized Cost of System* (LCOS), is expressed in euro per MWh and refers to the weighted average of electricity and hydrogen costs. We do not include the numerals of percentages lower than 1.5% in the bars for legibility. The figure title lists the following additional performance indices of the optimal solution. Although the main scenarios discussed in this paper include a zero CO₂ constraint, and therefore, the CO₂ emission factor is always zero, this index is stated in the title. Curtailment is reported next as a percentage of the primary generation of electricity. The shadow price of CO₂ is expressed in euros per ton. The delivered quantities and costs of the two energy services are expressed in TWh per year and euros per unit of energy, respectively. For hydrogen, a cost equivalence in euros per unit of mass is also indicated. The system cost minimization yields the LCOS, which is the equivalent objective function since the quantities of the delivered energy services are input parameters. Comparing the decomposition by technology of the three bars highlights the relative cost contribution. For example, in scenario A, solar requires only 21% of the LCOS while providing 36% of the dispatched electricity and 59% of the primary generation. Conversely, an auxiliary technology such as OCGT generates only 3% of

the dispatched electricity. Still, it requires an LCOS share of 3.6% for the OCGT plant itself, plus the shares of the methanation, DAC, CO₂ storage, and a sub-share of the hydrogen sub-system. The cost structure of each sub-system is provided in a following figure, but this first figure may already offer some general insights. The disaggregation of the LCOS in the costs of the two energy services, electricity and hydrogen, answers whether the district can competitively supply industrial plants. While the electricity and hydrogen delivered are input parameters, the primary generation and curtailment result from the system cost minimization. The primary generation compounded by the curtailment rate provides insights into the effective environmental impact of energy production. As recalled in the Introduction, LCA studies generally focus on the impact per unit of energy produced since the whole energy system analysis is out of their scope. Preliminary quantifications can be attained by comparing scenarios with different primary generation and curtailment values.

Fig. 7 shows the capacities of the installed technologies. Power capacities for the input and output are depicted in yellow and blue, respectively. The power scale is the top horizontal axis with MW as unit. For DAC, a technology with mass flow as output, the unit is ton of CO₂ per hour. The output of e-CH₄ refers to the link between the geological storage and the methane bus, and this is generally one order of magnitude larger than the output of the methanation plant itself (when appropriate, details of the e-CH₄ plant will be provided by an additional figure). The energy or mass storage capacities are reported as red bars, and their scale is the bottom horizontal axis with MWh or ton of CO₂ as unit. This scale is logarithmic. The red bars are labeled with the maximum duration of discharge, expressed in hours. This index is the ratio between the installed energy and power output capacities.

Fig. 8 depicts the hourly state of charge for the installed storage technologies. The vertical axis is in logarithmic scale. The legend reports the annual rotation rate of the installed storage capacity for each technology. This and the previous figure show the interplay of the annual rotation rate and maximum discharge in the system optimization for storage technologies. Technologies optimally configured with low discharge

rates tend to have high rotation rates and *vice versa*. This comparison should clarify why some studies fail to properly optimize renewable-based energy systems: they pre-assign non-optimal roles to storage technologies, such as setting batteries for long discharge and low rotation rate or electrolysis for short discharge and high rotation rate.

Fig. 9 shows the cost structure and price per unit of service delivered for each installed technology. The unitary cost is the sum of the following three components:

- CAPEX + FO&M, the investment annuity, and the fixed operations and management costs.
- VO&M, the variable operations and management costs.
- Input, the cost of the inputs. For example, the electrolysis input cost is the cost of the required electricity, and the input cost of methanation is the cost of the required hydrogen and CO₂.

Each unitary cost bar indicates the net capacity factor for the technology in its label. The net capacity factor results from the optimization and refers to the useful generation excluding curtailment. The average price per unit of service delivered is indicated as a black diamond. This average price is derived from the dual variables of the linear program. We notice that there are no active constraints on the minimum capacity of technologies in this scenario. Therefore, each installed technology satisfies equality between costs and revenues, i.e. cost-price parity (Brown and Reichenberg, 2021).

5.2 Results of scenarios A-H

We first quantify the system advantage of GPV by comparing the results of scenario A, Figs. 6—9, with those of scenarios B and C, Figs. 12—15 and 16—19, respectively. Additional results of scenario A in Figs. 10-11 will be commented in the following. This comparison shows that vetoing GPV increases LCOS by 15—25% and storage capacities by 16—20%. Hydrogen produced without GPV has an extra cost of 14—21%

relative to scenario A. The analysis of the primary generation and curtailment is significant. In scenario A, the primary generation is 13.2 TWh/y and the curtailment rate is 12%, i.e. 1.6 TWh/y are curtailed. This quantity may be considered physiological, particularly in light of our model's worst-case assumptions for renewables. Scenario C, instead, requires a primary generation of 13 TWh/y and a curtailment rate of 26%, i.e. 3.4 TWh/y are curtailed, double of scenario A. Analysis of the storage capacities offers another example of the system advantage of GPV. Scenario A balances supply and demand with a minimal contribution of batteries. Wind and solar supply directly 77% of the demand, PHS contributes 20%, and OCGT supplies the remaining few percentage points fueled by e-CH₄, plus a minimal and non-significant amount of batteries. Scenario B, instead, requires 11% of the demand to be covered by batteries installed with a power output of 0.8 GW. Scenario C reduces storage requirements relative to scenario B, but this is accomplished by increasing reliance on wind. Henceforth, the lower performance of solar rooftop in scenario C is balanced out by another efficient land-based renewable source.

The system advantage of onshore wind is quantified by comparing the results of scenario D, Figs. 20—23, with those described above. Without onshore wind, the system cost increases, GPV is the main primary source, and nuclear enters the optimal mix.

If both land-based renewables, GPV and onshore wind, are vetoed, then the system cost increases further and so does the primary share of nuclear, see results of scenarios E and F, Figs. 24—27 and 28—31, respectively. Oversizing solar rooftop is induced by vetoing onshore wind since the increased seasonal imbalance causes an increase in the least efficient storage technology, i.e. methanation.

Scenario G, Figs. 32—34, assesses the nuclear capacity required to supply the two energy services by this source only. The required capacity is 1486 MW_e, which is within the range of new commercial reactors, such as the AP1000 with 1117 MW_e and the EPR with 1660 MW_e. Only in this scenario does nuclear attain its maximum value of 90% as optimal CF. In the other scenarios where nuclear enters the optimal mix, scenarios D—

F, its CF is 65—77%. Our results on the nuclear CF with renewable competition align with that of IEA (Bouckaert et al., 2021). This fact can be explained by observing the hourly price formation of electricity. Fig. 11 illustrates the duration curve of the hourly prices in scenario A. Similar curves hold in the other scenarios with large contributions of wind and solar, and for simplicity, here we omit them (full results are available in the Git-Hub repository Moccia (2024)). We observe that the electricity price is very low three-fourths of the time. This share coincides with that of wind and solar in the dispatched electricity of scenario A, see the mid bar in Fig. 6. The remaining fourth of the time exhibits increasing prices depending on the marginal cost of storage. Thus, the average annual price remains low although some hours face high prices to remunerate storage sub-systems. Fig. 9 indicates that scenario A’s most expensive electricity supply is by OCGT with a net CF of 7% and an average price of 250 €/MWh. Although this technology is costly, it is cheaper than a hypothetical nuclear with CF of 7%, which would cost 1000 €/MWh. This is why nuclear does not enter the optimal mix in scenarios A—C, and it displays lower than maximum CF when competing with partially vetoed renewables. The marginal cost of nuclear, albeit low, is not near zero as for wind and solar. This system dynamics is well known and leads some authors to be skeptical of a relevant role of nuclear in the first half of this century, see e.g. Haywood et al. (2023).

Results of scenario H, Figs. 35—38, illustrate the impact of generalized vetoes. Installed solar rooftop amounts to ~16 GW, four times the installed GPV in scenario A. Similar oversizing occurs in storage. While scenario A requires ~0.8 GW of PHS and a negligible capacity of batteries, scenario H commands 3.2 GW of batteries, four times the PHS in scenario A. Comparing the state-of-charge of long-term storage among scenarios, Fig. 38 *vs.* Fig. 9, the performance worsening with increasing vetoes is self-evident. For example, the e-CH₄ storage sub-system halves the rotation rate and increases capacity by one order of magnitude. In absolute terms, scenario A requires only 0.25 TWh of e-CH₄ storage *vs.* 2.2 TWh in scenario H. Moreover, the CO₂ shadow price almost doubled between scenarios A and H.

**Primary generation, delivered electricity, and LCOS values and shares at 0 gCO₂/kWh, curtailment 12%, CO₂ shadow price 265 €/t
Delivered 8.76 TWh/y of electricity at 56.5 €/MWh and 2.19 TWh/y of H₂ at 46.7 €/MWh = 1.40 €/kg**

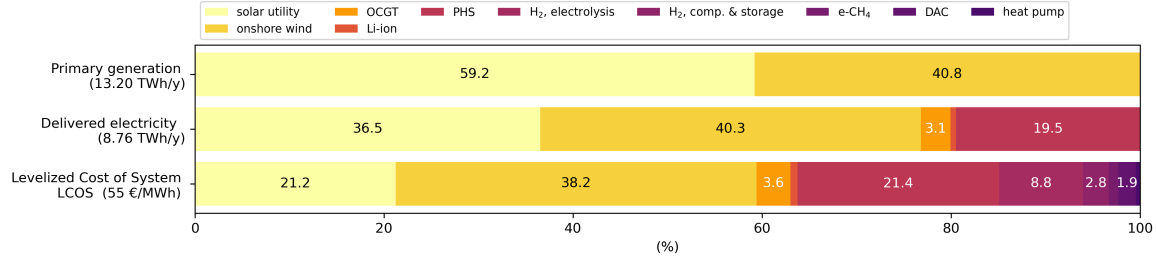


Figure 6: Scenario A, no vetoes, main indices.

Installed capacities:
power or mass flow (top axis, linear scale)
and energy or mass (bottom axis, log scale,
and in parenthesis the maximum discharge duration in hours, rounded to the nearest integer)

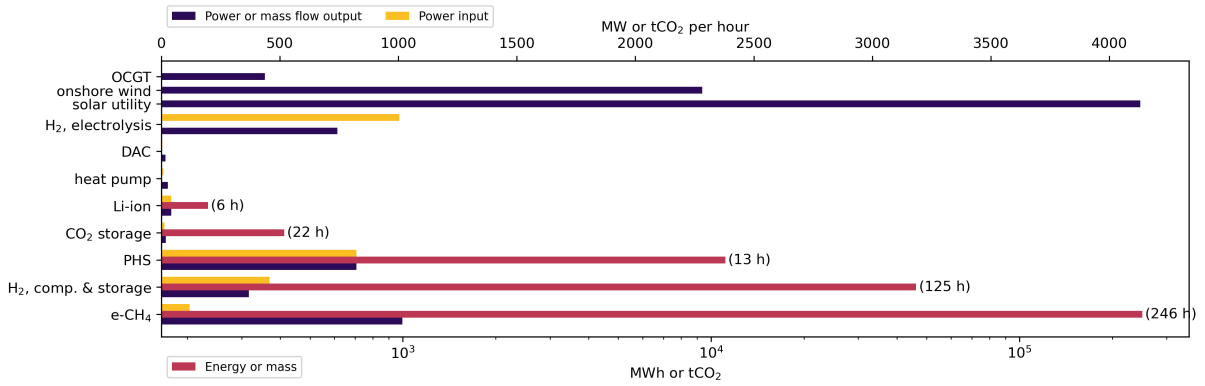


Figure 7: Scenario A, no vetoes, installed capacities.

Besides the higher system cost of this oversizing, scenario H likely presents a significant increase in life-cycle environmental impacts. In scenario H, the primary generation is 16.6 TWh/y and curtailment 54% vs. 13.2 TWh/y and 12%, respectively, in scenario A. Thus, scenario H requires +73% overgeneration relative to scenario A. This systemic penalty of exclusive solar rooftop would be multiplicative of that computed per unit of energy produced. Adding the impacts of storage hints that exclusive solar rooftop would more than double the life-cycle impacts relative to an optimal mix with land-based wind and solar.

Tab. 2 and Fig. 39 synthesize vetoes and primary generation shares, and LCOS, respectively, for scenarios A—H.

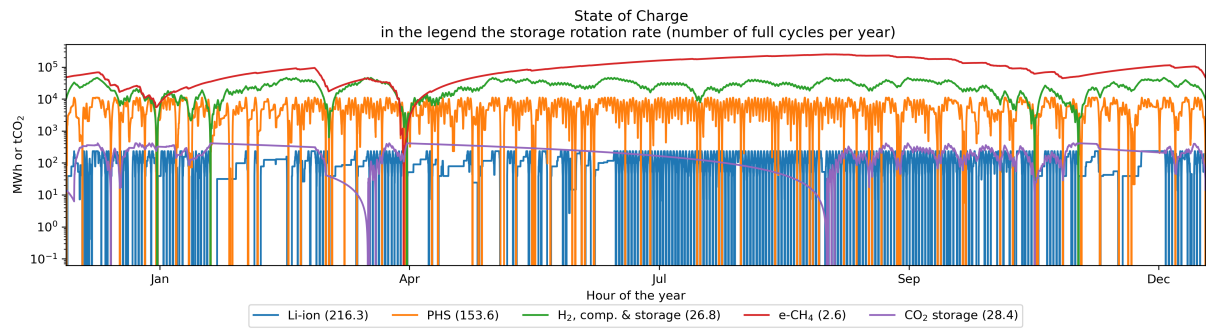


Figure 8: Scenario A, no vetoes, state of charge of storage.

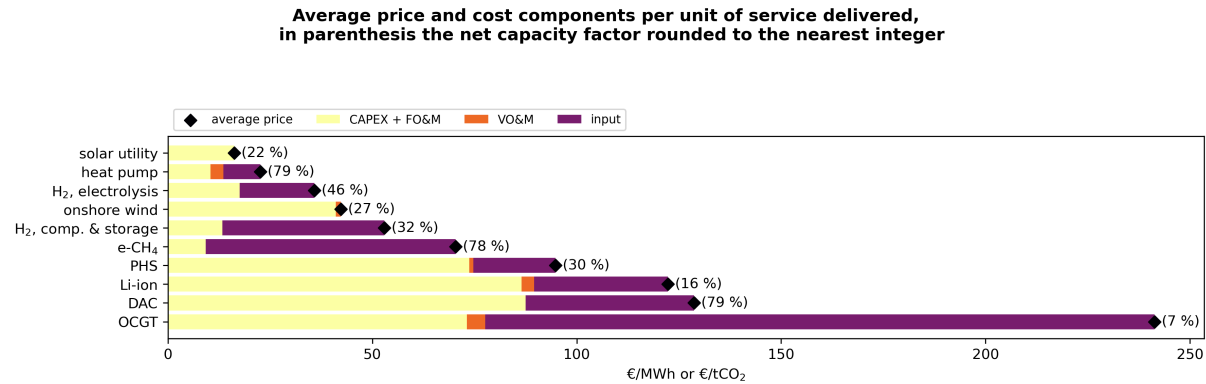


Figure 9: Scenario A, no vetoes, average price and cost structure.

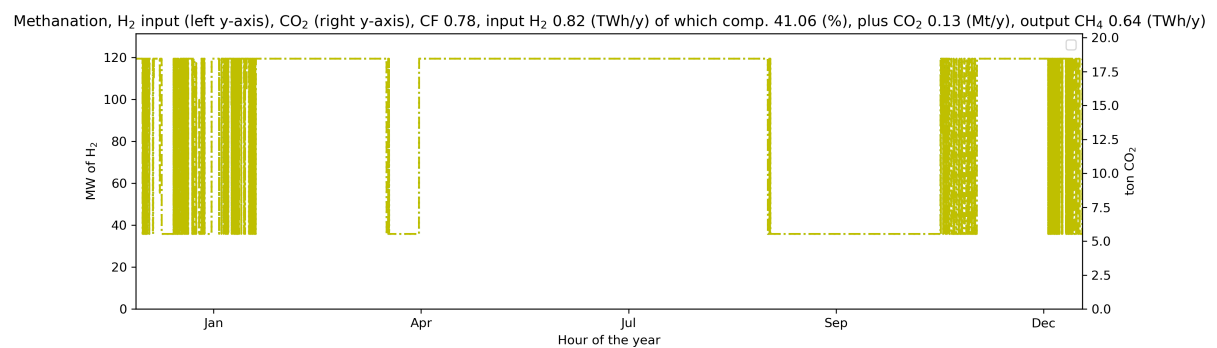


Figure 10: Scenario A, no vetoes, main indices and hourly capacity factors of the methanation plant.

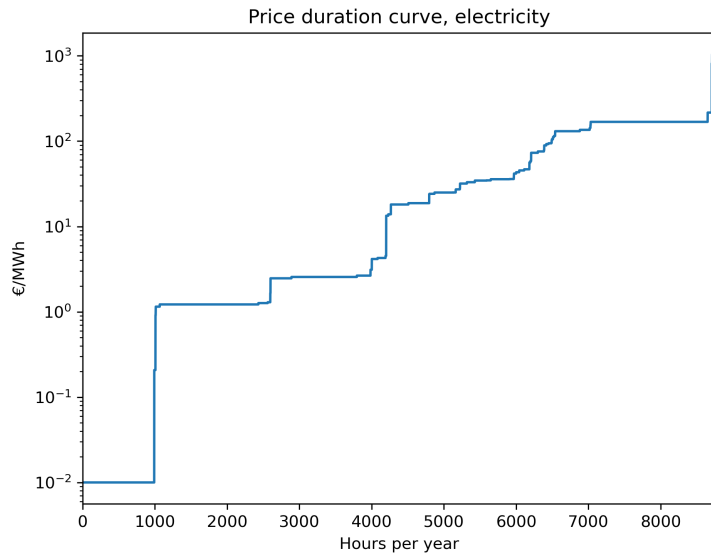


Figure 11: Scenario A, duration curve of the hourly electricity prices.

**Primary generation, delivered electricity, and LCOS values and shares at 0 gCO₂/kWh, curtailment 11%, CO₂ shadow price 291 €/t
Delivered 8.76 TWh/y of electricity at 64.9 €/MWh and 2.19 TWh/y of H₂ at 53.1 €/MWh = 1.59 €/kg**

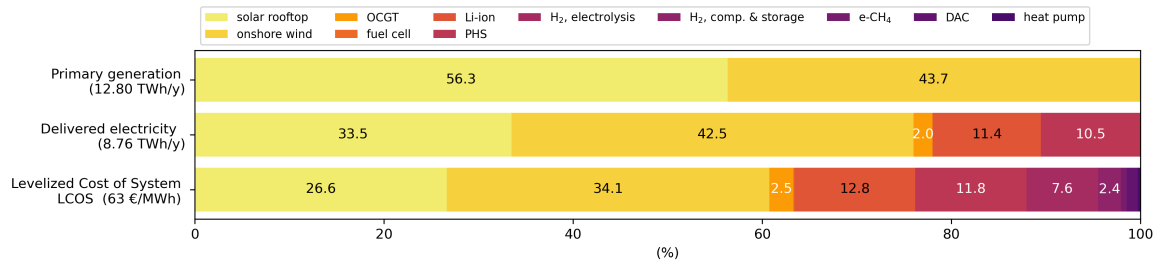


Figure 12: Scenario B, veto on ground-based PV, solar rooftop with high CF, main indices.

**Installed capacities:
power or mass flow (top axis, linear scale)
and energy or mass (bottom axis, log scale,
and in parenthesis the maximum discharge duration in hours, rounded to the nearest integer)**

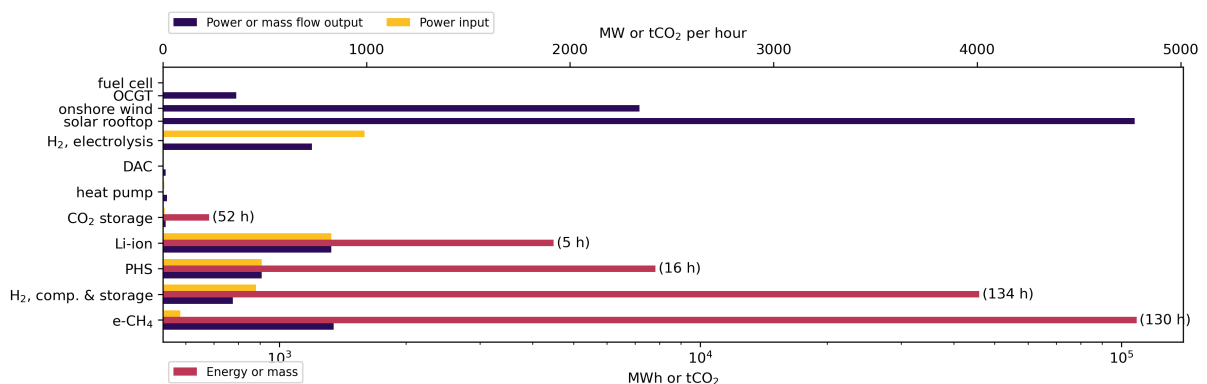


Figure 13: Scenario B, veto on ground-based PV, solar rooftop with high CF, installed capacities.

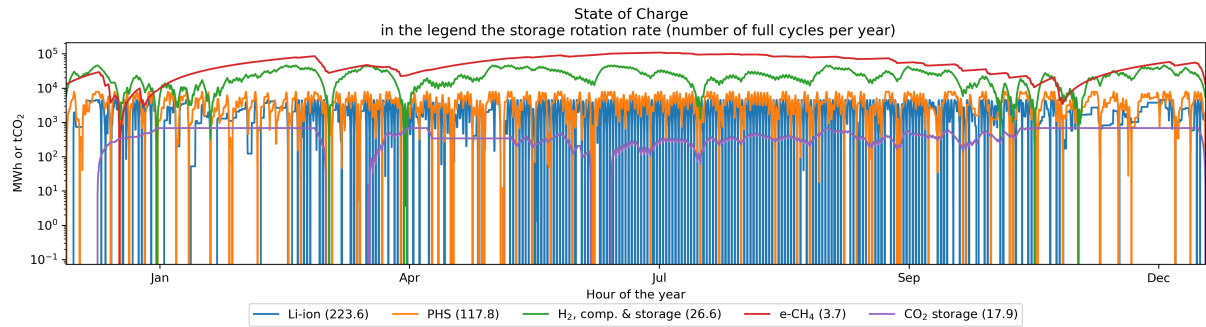


Figure 14: Scenario B, veto on ground-based PV, state of charge of storage.

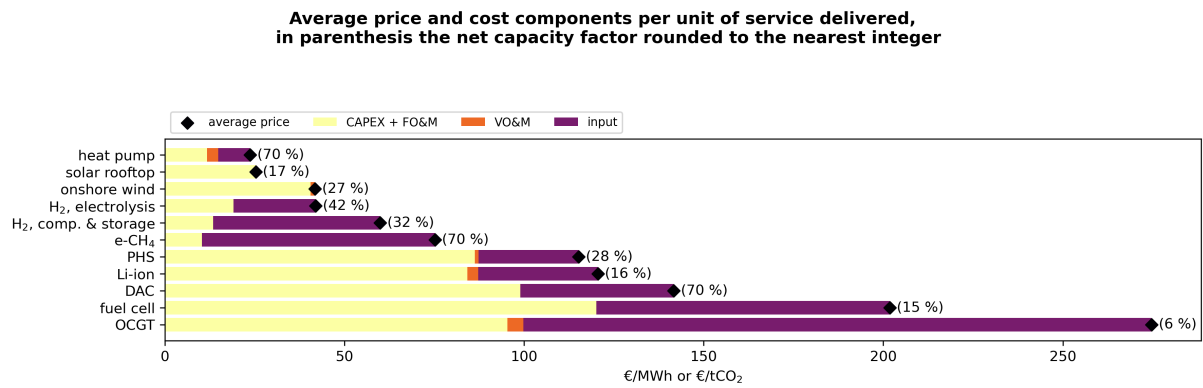


Figure 15: Scenario B, veto on ground-based PV, average price and cost structure.

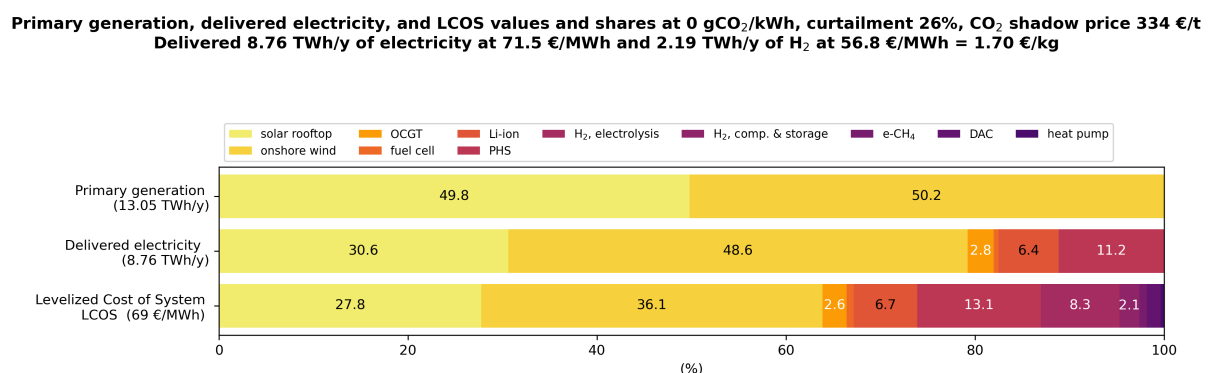


Figure 16: Scenario C, veto on ground-based PV, solar rooftop with low CF, main indices.

Installed capacities:
power or mass flow (top axis, linear scale)
and energy or mass (bottom axis, log scale,
and in parenthesis the maximum discharge duration in hours, rounded to the nearest integer)

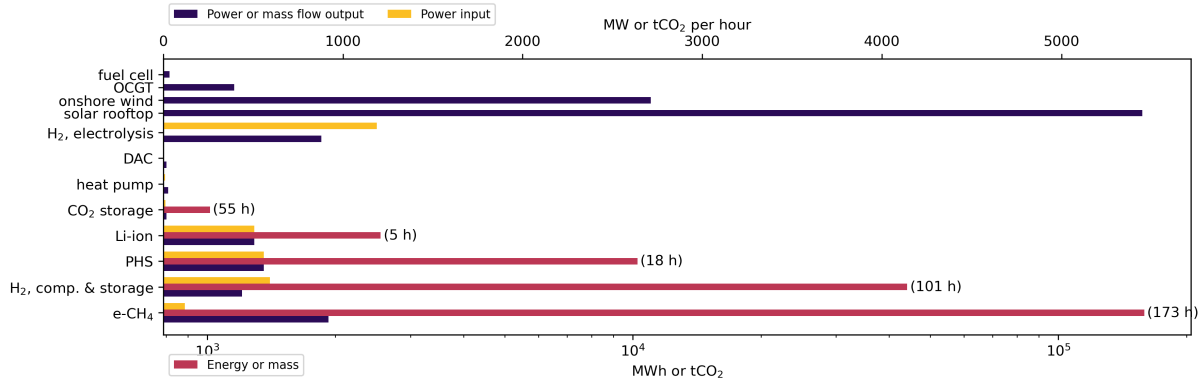


Figure 17: Scenario C, veto on ground-based PV, solar rooftop with low CF, installed capacities.

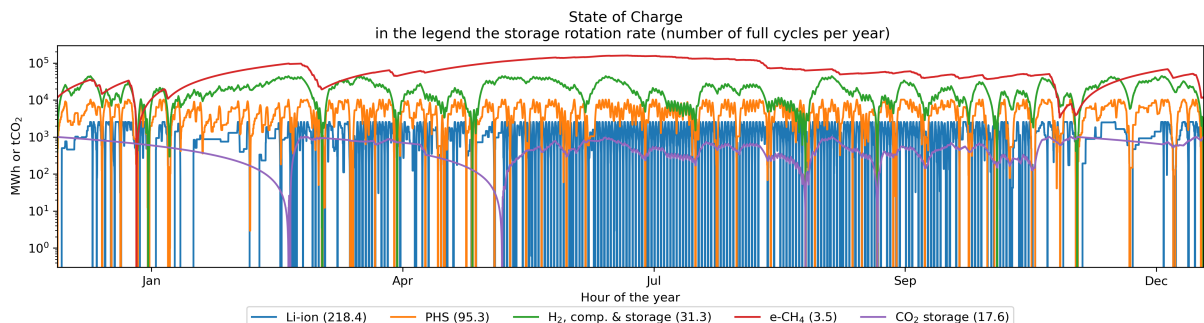


Figure 18: Scenario C, veto on ground-based PV, solar rooftop with low CF, state of charge of storage.

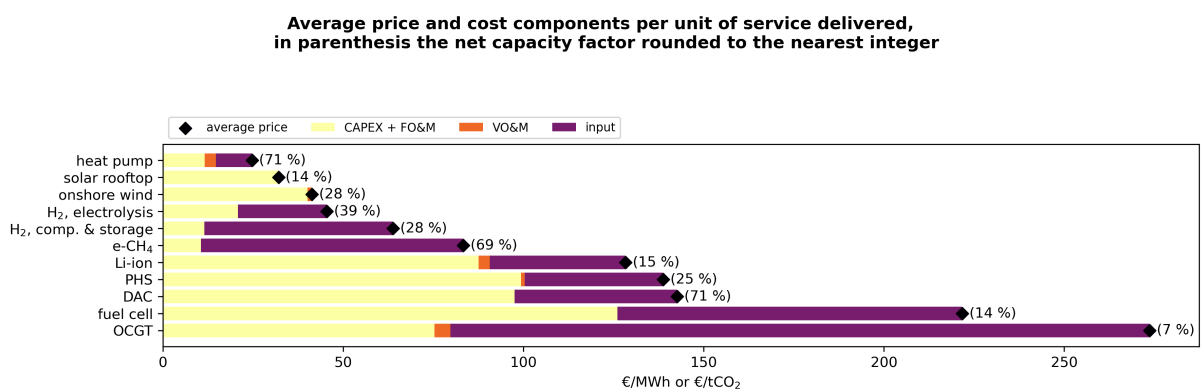


Figure 19: Scenario C, veto on ground-based PV, solar rooftop with low CF, average price and cost structure.

**Primary generation, delivered electricity, and LCOS values and shares at 0 gCO₂/kWh, curtailment 26%, CO₂ shadow price 328 €/t
Delivered 8.76 TWh/y of electricity at 79.7 €/MWh and 2.19 TWh/y of H₂ at 78.5 €/MWh = 2.36 €/kg**

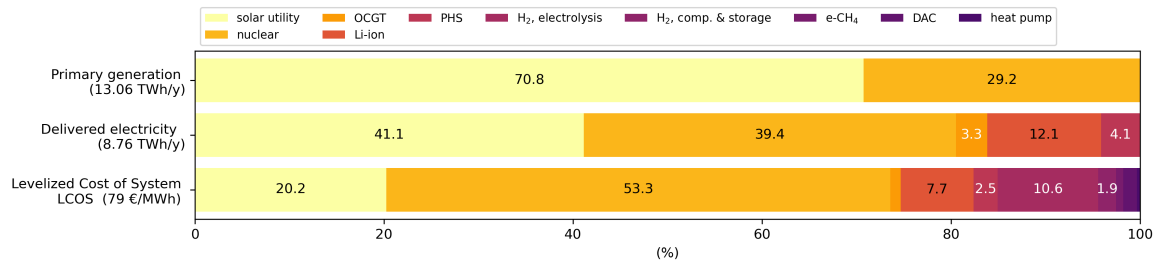


Figure 20: Scenario D, veto against onshore wind, main indices.

**Installed capacities:
power or mass flow (top axis, linear scale)
and energy or mass (bottom axis, log scale,
and in parenthesis the maximum discharge duration in hours, rounded to the nearest integer)**

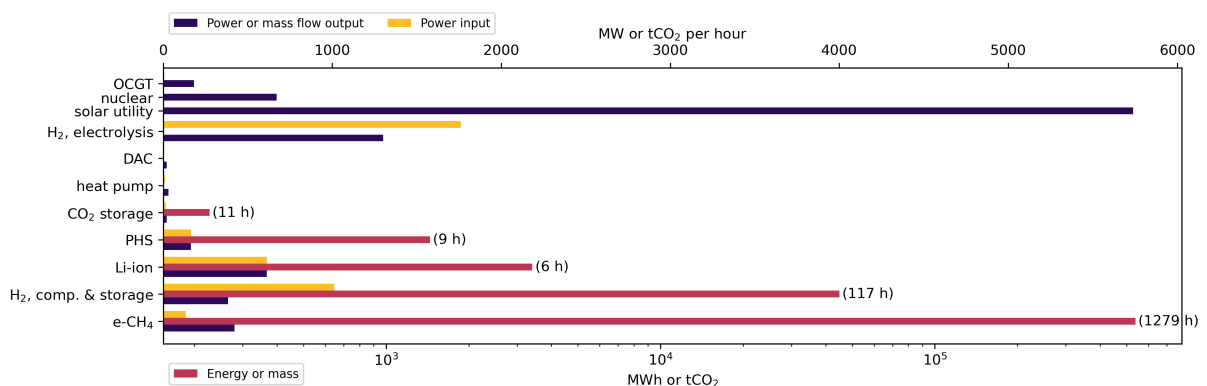


Figure 21: Scenario D, veto against onshore wind, installed capacities.

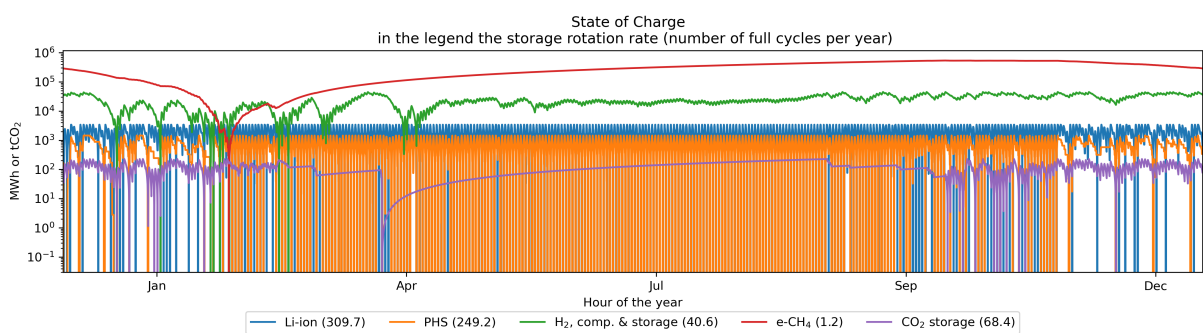


Figure 22: Scenario D, veto against onshore wind, state of charge of storage.

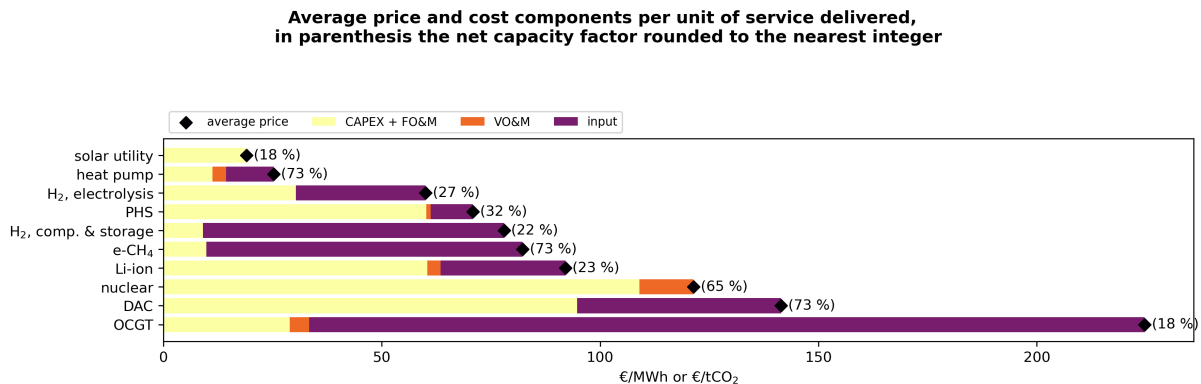


Figure 23: Scenario D, veto against onshore wind, average price and cost structure.

**Primary generation, delivered electricity, and LCOS values and shares at 0 gCO₂/kWh, curtailment 11%, CO₂ shadow price 385 €/t
Delivered 8.76 TWh/y of electricity at 82.7 €/MWh and 2.19 TWh/y of H₂ at 90.5 €/MWh = 2.71 €/kg**

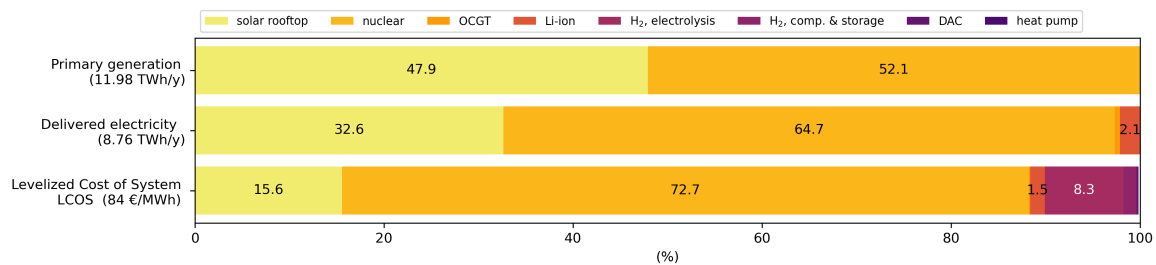


Figure 24: Scenario E, vetoes on GPV and onshore wind, solar rooftop with high CF as in scenario B, main indices.

**Installed capacities:
power or mass flow (top axis, linear scale)
and energy or mass (bottom axis, log scale,
and in parenthesis the maximum discharge duration in hours, rounded to the nearest integer)**

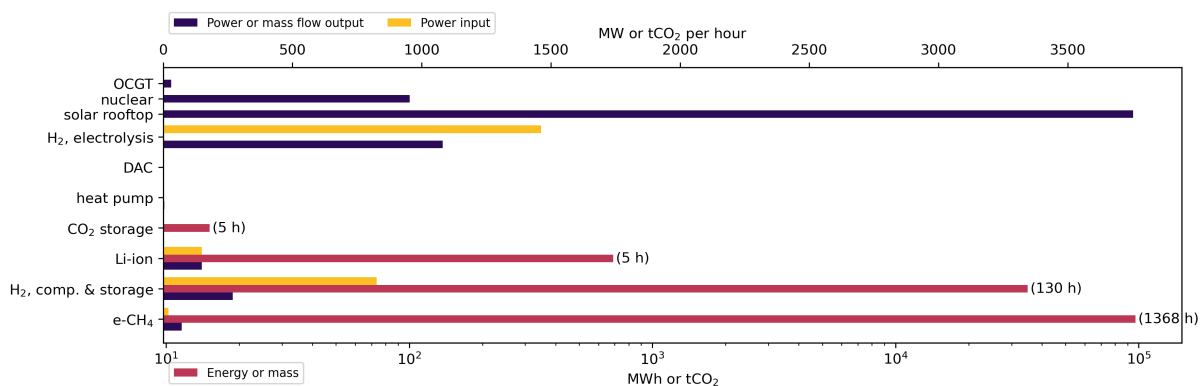


Figure 25: Scenario E, vetoes on GPV and onshore wind, solar rooftop with high CF as in scenario B, installed capacities.

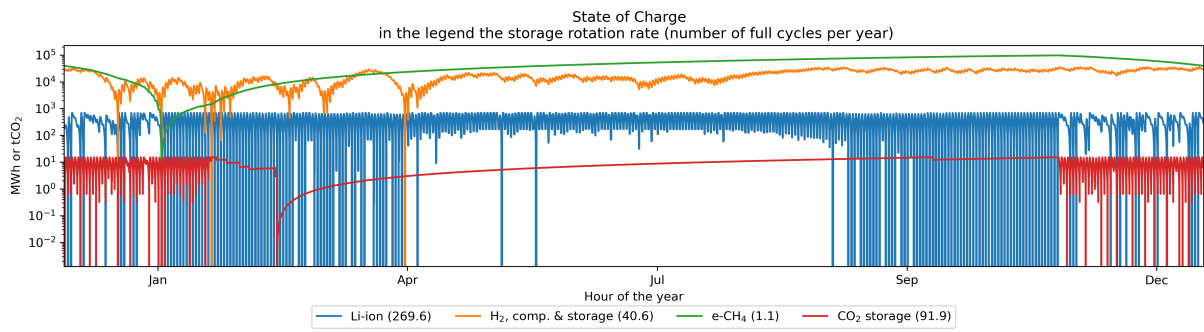


Figure 26: Scenario E, vetoes on GPV and onshore wind, solar rooftop with high CF as in scenario B, state of charge of storage.

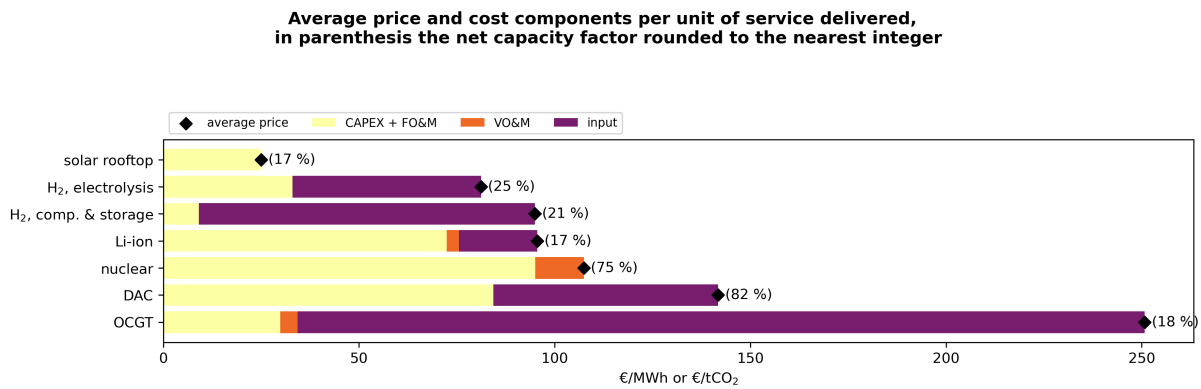


Figure 27: Scenario E, vetoes on GPV and onshore wind, solar rooftop with high CF as in scenario B, average price and cost structure.

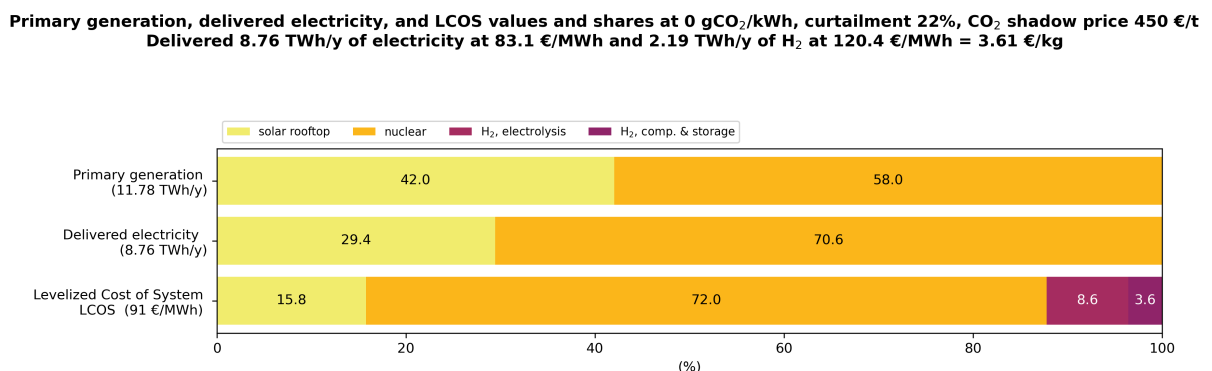


Figure 28: Scenario F, vetoes on GPV and onshore wind, solar rooftop with low CF as in scenario C, main indices.

Installed capacities:
power or mass flow (top axis, linear scale)
and energy or mass (bottom axis, log scale,
and in parenthesis the maximum discharge duration in hours, rounded to the nearest integer)

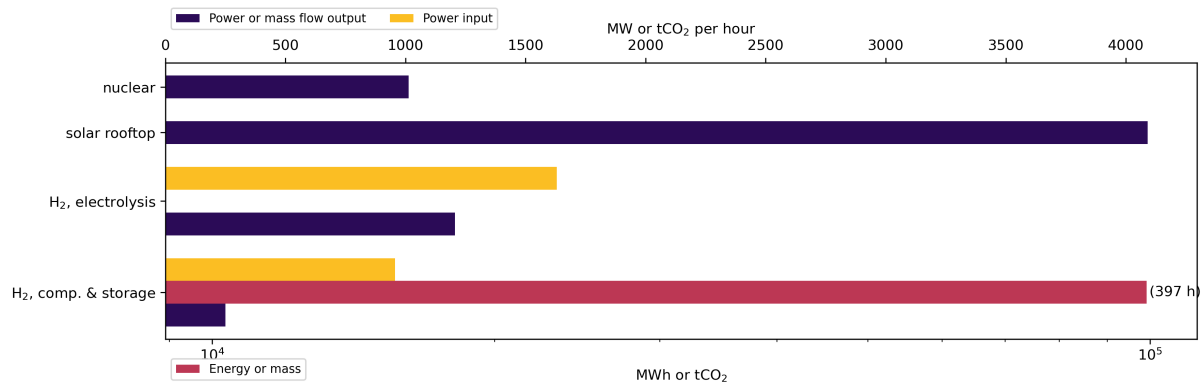


Figure 29: Scenario F, vetoes on GPV and onshore wind, solar rooftop with low CF as in scenario C, installed capacities.

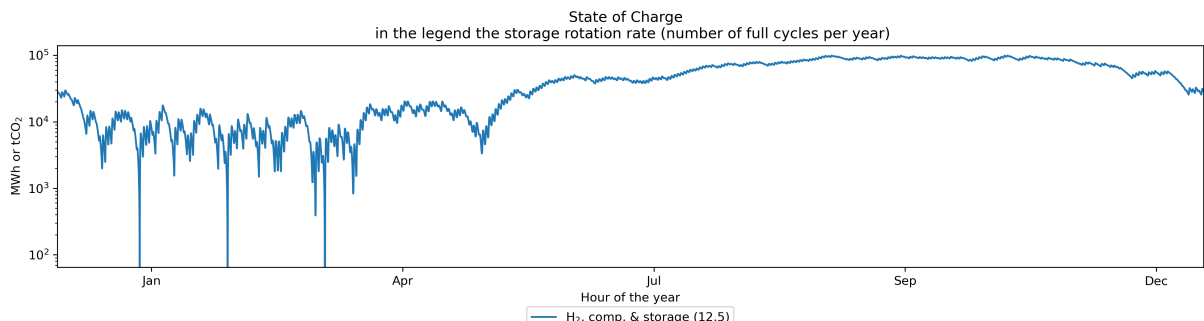


Figure 30: Scenario F, vetoes on GPV and onshore wind, solar rooftop with low CF as in scenario C, state of charge of storage.

**Average price and cost components per unit of service delivered,
in parenthesis the net capacity factor rounded to the nearest integer**

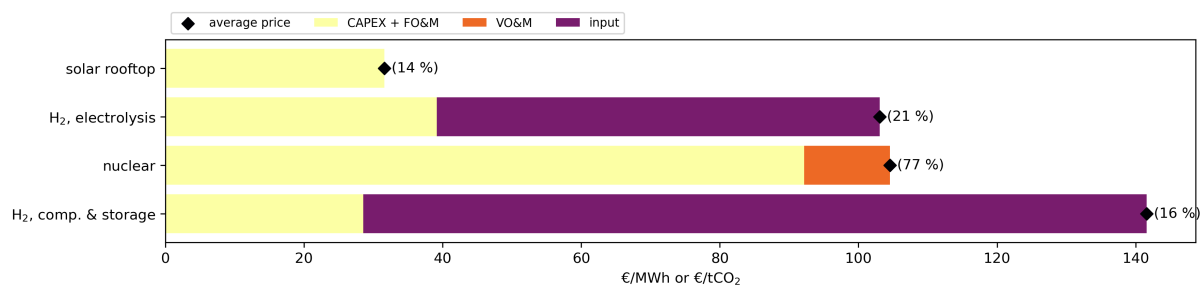


Figure 31: Scenario F, vetoes on GPV and onshore wind, solar rooftop with low CF as in scenario C, average price and cost structure.

**Primary generation, delivered electricity, and LCOS values and shares at 0 gCO₂/kWh, curtailment 0%, CO₂ shadow price 91 €/t
Delivered 8.76 TWh/y of electricity at 91.2 €/MWh and 2.19 TWh/y of H₂ at 132.3 €/MWh = 3.97 €/kg**

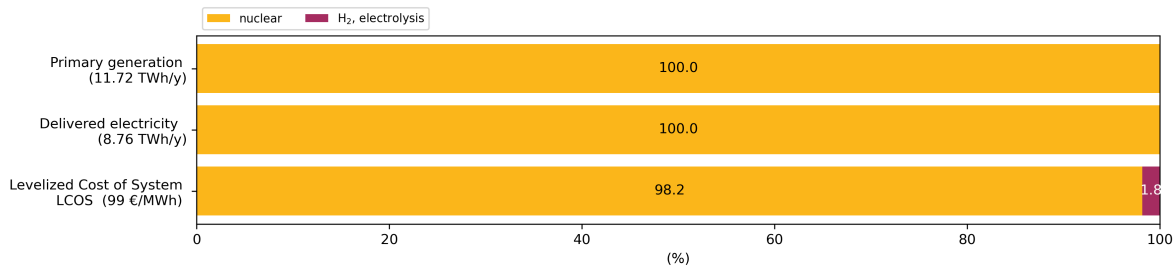


Figure 32: Scenario G, only nuclear, main indices.

**Installed capacities:
power or mass flow (top axis, linear scale)
and energy or mass (bottom axis, log scale,
and in parenthesis the maximum discharge duration in hours, rounded to the nearest integer)**

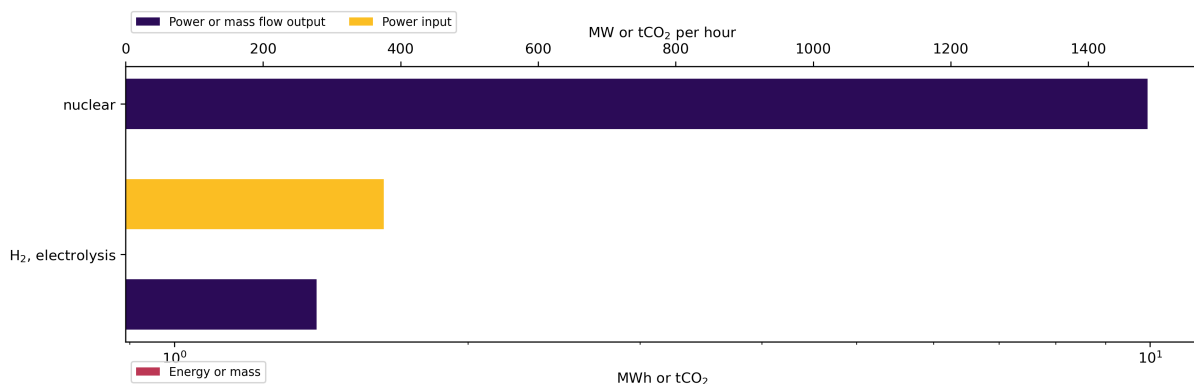


Figure 33: Scenario G, only nuclear, installed capacities.

**Average price and cost components per unit of service delivered,
in parenthesis the net capacity factor rounded to the nearest integer**

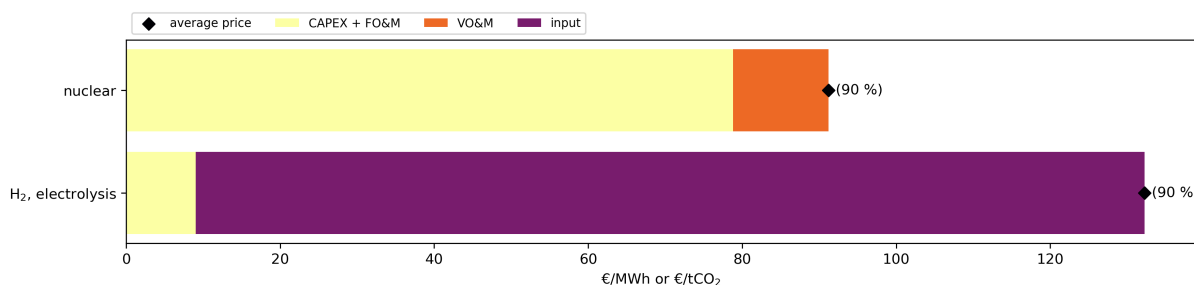


Figure 34: Scenario G, only nuclear, average price and cost structure.

**Primary generation, delivered electricity, and LCOS values and shares at 0 gCO₂/kWh, curtailment 54%, CO₂ shadow price 493 €/t
Delivered 8.76 TWh/y of electricity at 120.6 €/MWh and 2.19 TWh/y of H₂ at 114.7 €/MWh = 3.44 €/kg**

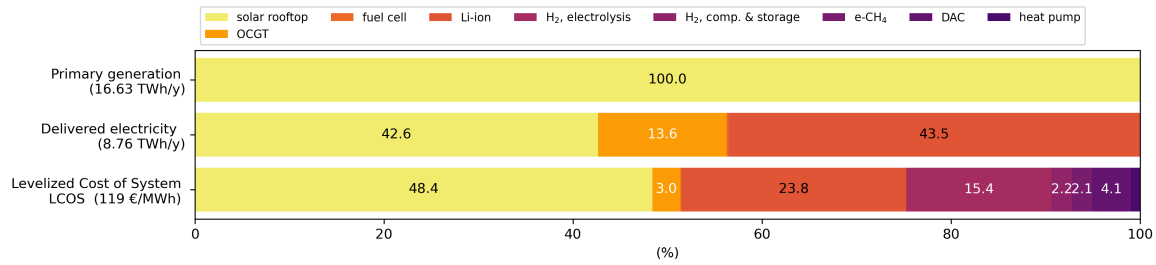


Figure 35: Scenario H, vetoes on land-based renewables and nuclear, solar rooftop with low CF as in scenario C, main indices.

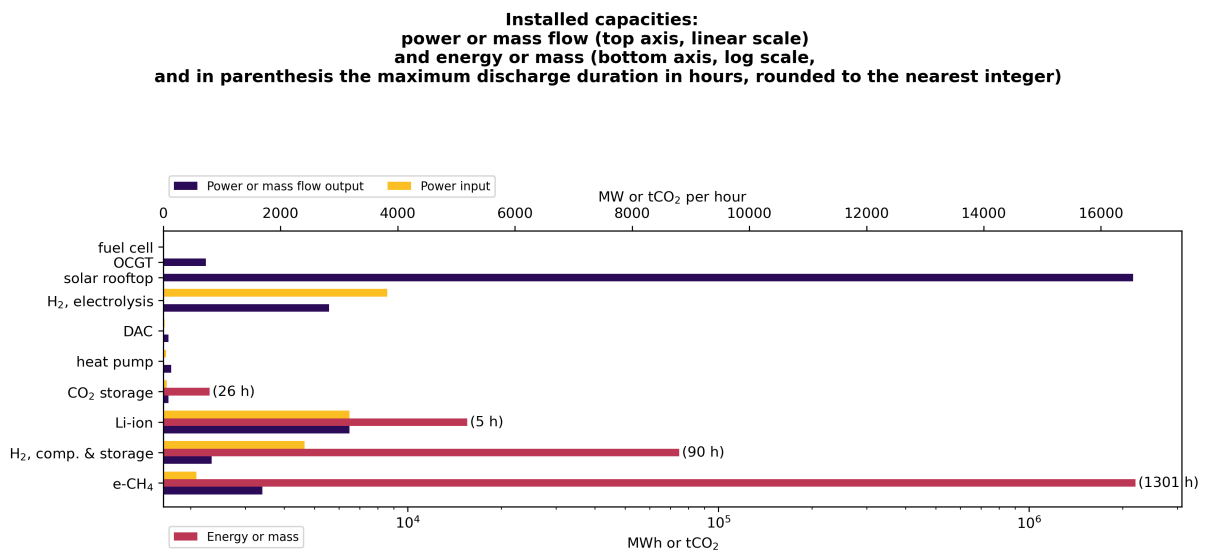


Figure 36: Scenario H, vetoes on land-based renewables and nuclear, solar rooftop with low CF as in scenario C, installed capacities.

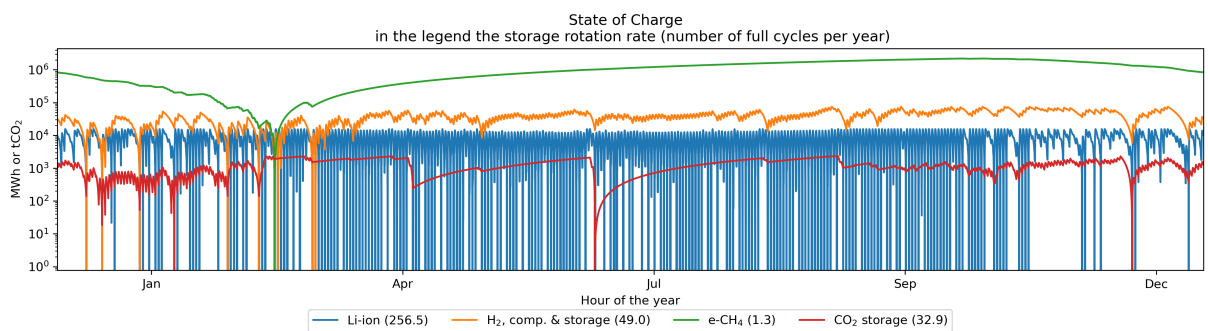


Figure 37: Scenario H, vetoes on land-based renewables and nuclear, solar rooftop with low CF as in scenario C, state of charge of storage.

**Average price and cost components per unit of service delivered,
in parenthesis the net capacity factor rounded to the nearest integer**

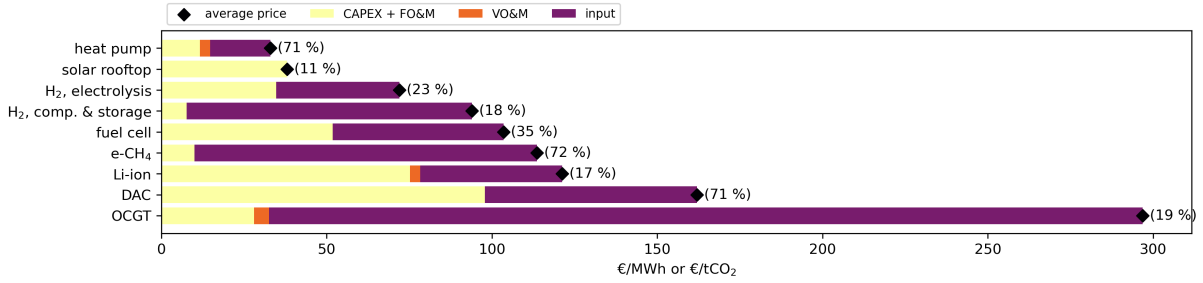


Figure 38: Scenario H, vetoes on land-based renewables and nuclear, solar rooftop with low CF as in scenario C, average price and cost structure.

Scenario	Solar utility	Solar rooftop high CF	Solar rooftop low CF	Onshore wind	Nuclear
A	✓59	○	○	✓41	○
B	✗	✓56	○	✓44	○
C	✗	✗	✓50	✓50	○
D	✓71	○	○	✗	✓29
E	✗	✓48	○	✗	✓52
F	✗	✗	✓42	✗	✓58
G	✗	✗	✗	✗	✓100
H	✗	✗	✓100	✗	✗

Table 2: Synthesis of vetoes and shares of primary technologies in scenarios A—H. A vetoed technology is indicated by ✗. The symbol ○ designates a technology that, although not vetoed in a scenario, it is not activated for lack of competitiveness. A technology that is activated is reported by the symbol ✓with its percentage in the primary generation (rounded to the nearest integer).

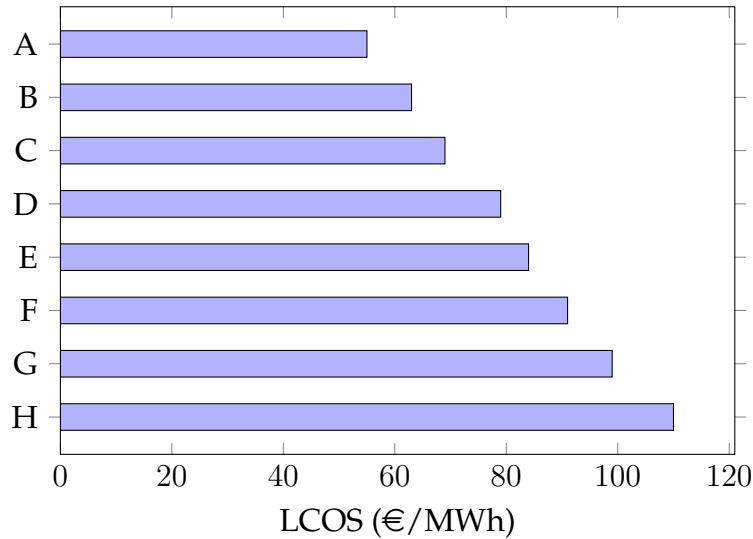


Figure 39: Levelized Cost of System of scenarios A—H

5.3 Results of scenarios \dot{A} — \dot{H}

Tab. 3 and Fig. 40 report the vetoes and primary shares, and LCOS of scenarios \dot{A} — \dot{H} , respectively, with the same format as Tab. 2 and Fig. 39 for scenarios A—H. The realistic difference in discount rates between renewables and nuclear yields a non significant role of the latter technology. Among the scenarios where nuclear must compete with renewables, it enters the optimal mix only in scenario \dot{F} , but with a primary share of $\sim 1\%$. In fact, scenario \dot{H} , where nuclear is vetoed, attains an LCOS almost equal to scenario \dot{F} . Therefore, a veto on nuclear under technology-specific discount rates should not be considered burdensome in South Italy. We further observe that the wind and solar primary shares are similar between the scenario sets \dot{A} — \dot{H} and A—H. The LCOS ratio between scenarios \dot{H} and \dot{A} is 2.3. This value is similar to the LCOS ratio between scenarios H and A. We, therefore, conclude that the more favorable discount rate in scenarios \dot{A} — \dot{H} does not significantly alter the previously discussed relative burden of the vetoes against land-based wind and solar.

Further insights can be drawn by comparing Figs. 41—48 that report the results of scenarios \dot{A} and \dot{H} with those previously presented for scenarios A and H. The overgeneration of scenario \dot{A} is slightly less than in scenario A, whereas the overgeneration of scenario \dot{H} worsens relative to scenario H. The overgeneration of scenario \dot{H} is 80% larger than in scenario \dot{A} . Systemic worsening can be appreciated by comparing installed capacities of primary generation and storage (Fig. 42 vs. Fig. 46), rotation rates of storage (Fig. 43 vs. Fig. 47), and net capacity factors of sub-systems (Fig. 44 vs. Fig. 48). Therefore, also under favorable financing conditions, a scenario that excludes land-based wind and solar yields a very large overgeneration. This result is systemic, and more favorable cost assumptions do not attenuate it. On the contrary, it may be concluded that the lower the cost of solar rooftop, the larger the overgeneration would be.

Scenario	Solar utility	Solar rooftop high CF	Solar rooftop low CF	Onshore wind	Nuclear
\dot{A}	✓60	○	○	✓40	○
\dot{B}	✗	✓59	○	✓41	○
\dot{C}	✗	✗	✓53	✓47	○
\dot{D}	✓100	○	○	✗	○
\dot{E}	✗	✓100	○	✗	○
\dot{F}	✗	✗	✓99	✗	✓1
\dot{G}	✗	✗	✗	✗	✓100
\dot{H}	✗	✗	✓100	✗	✗

Table 3: Synthesis of vetoes and shares of primary technologies in scenarios \dot{A} — \dot{H} . A vetoed technology is indicated by \times . The symbol \circ designates a technology that, although not vetoed in a scenario, it is not activated for lack of competitiveness. A technology that is activated is reported by the symbol ✓ with its percentage in the primary generation (rounded to the nearest integer).

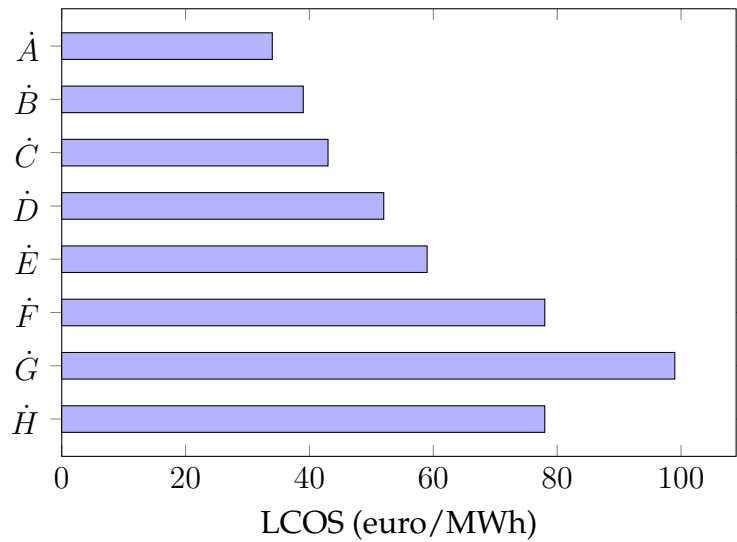


Figure 40: Levelized Cost of System of scenarios \dot{A} — \dot{H}

**Primary generation, delivered electricity, and LCOS values and shares at 0 gCO₂/kWh, curtailment 13%, CO₂ shadow price 142 €/t
Delivered 8.76 TWh/y of electricity at 34.7 €/MWh and 2.19 TWh/y of H₂ at 32.8 €/MWh = 0.99 €/kg**

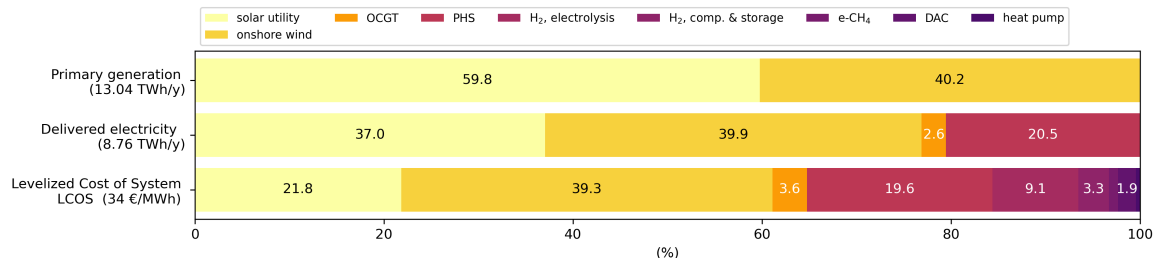


Figure 41: Scenario \dot{A} , technology-specific discount rates, no vetoes, main indices.

Installed capacities:
power or mass flow (top axis, linear scale)
and energy or mass (bottom axis, log scale,
and in parenthesis the maximum discharge duration in hours, rounded to the nearest integer)

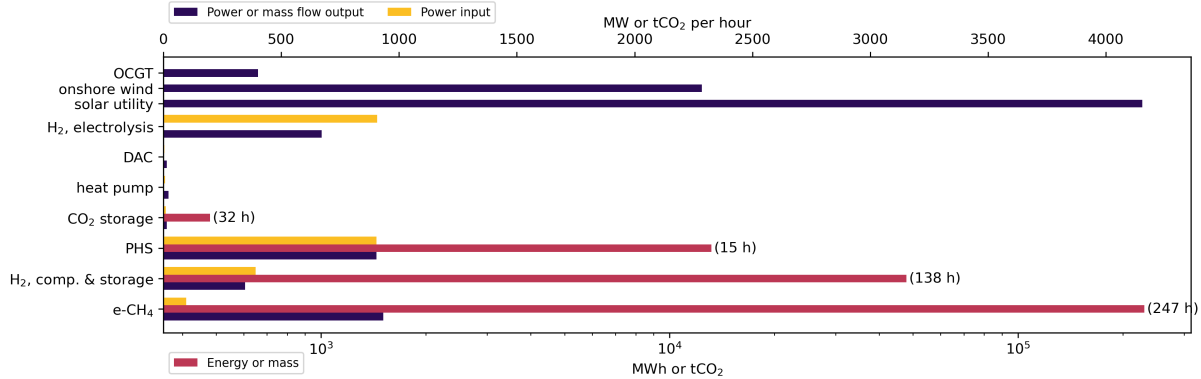


Figure 42: Scenario \dot{A} , technology-specific discount rates, no vetoes, installed capacities.

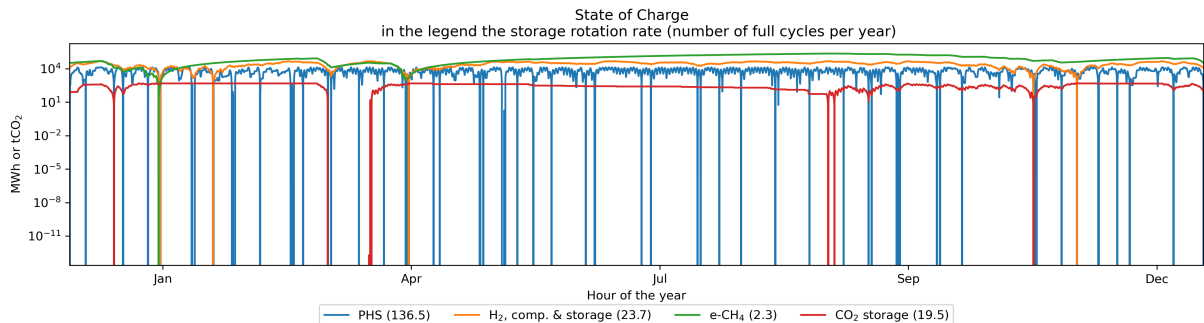


Figure 43: Scenario \dot{A} , technology-specific discount rates, no vetoes, state of charge of storage.

**Average price and cost components per unit of service delivered,
in parenthesis the net capacity factor rounded to the nearest integer**

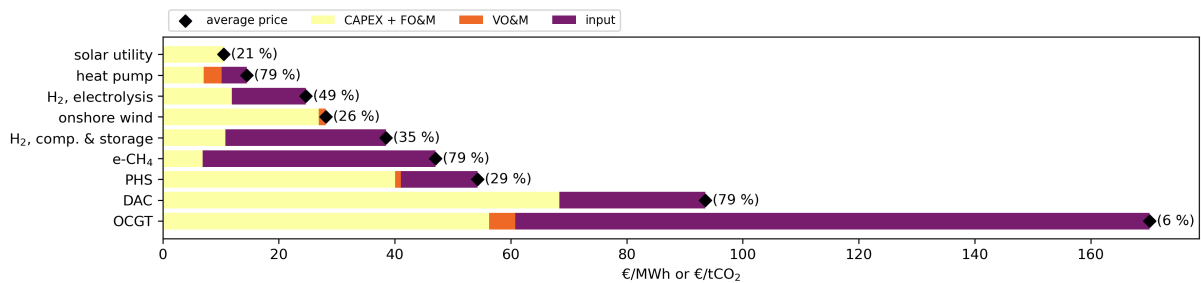


Figure 44: Scenario \dot{A} , technology-specific discount rates, no vetoes, average price and cost structure.

**Primary generation, delivered electricity, and LCOS values and shares at 0 gCO₂/kWh, curtailment 59%, CO₂ shadow price 307 €/t
Delivered 8.76 TWh/y of electricity at 77.9 €/MWh and 2.19 TWh/y of H₂ at 76.7 €/MWh = 2.30 €/kg**

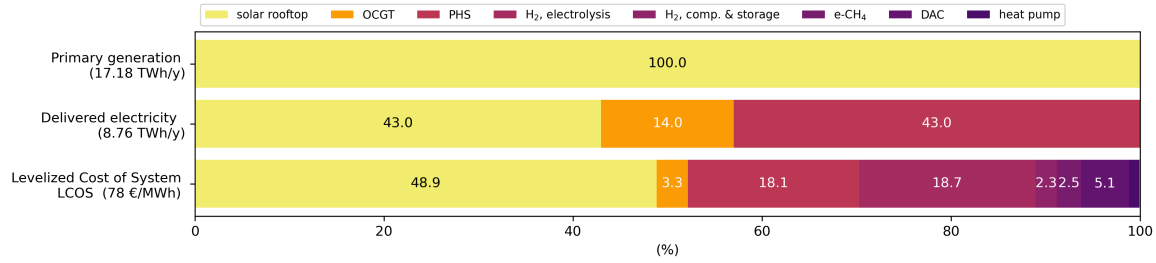


Figure 45: Scenario \dot{H} , technology-specific discount rates, vetoes on land-based renewables and nuclear, solar rooftop with low CF as in Scenario C, main indices.

**Installed capacities:
power or mass flow (top axis, linear scale)
and energy or mass (bottom axis, log scale,
and in parenthesis the maximum discharge duration in hours, rounded to the nearest integer)**

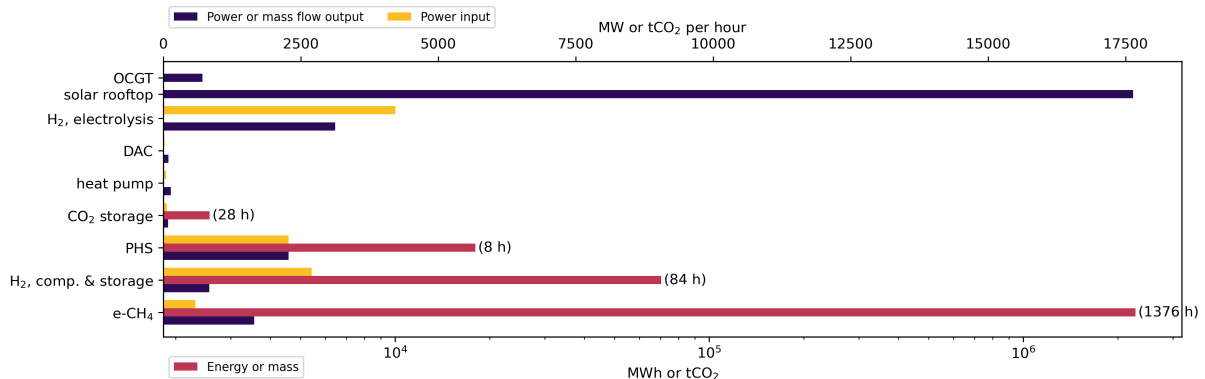


Figure 46: Scenario \dot{H} , technology-specific discount rates, vetoes on land-based renewables and nuclear, solar rooftop with low CF as in Scenario C, installed capacities.

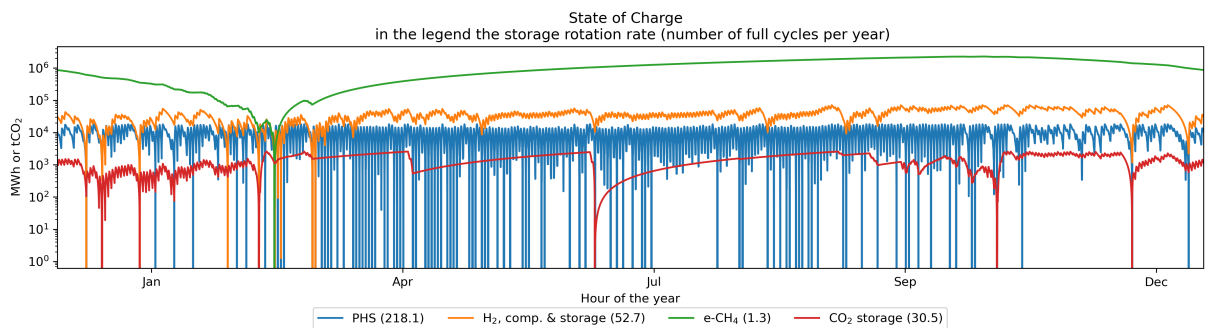


Figure 47: Scenario \dot{H} , technology-specific discount rates, vetoes on land-based renewables and nuclear, solar rooftop with low CF as in scenario C, state of charge of storage.

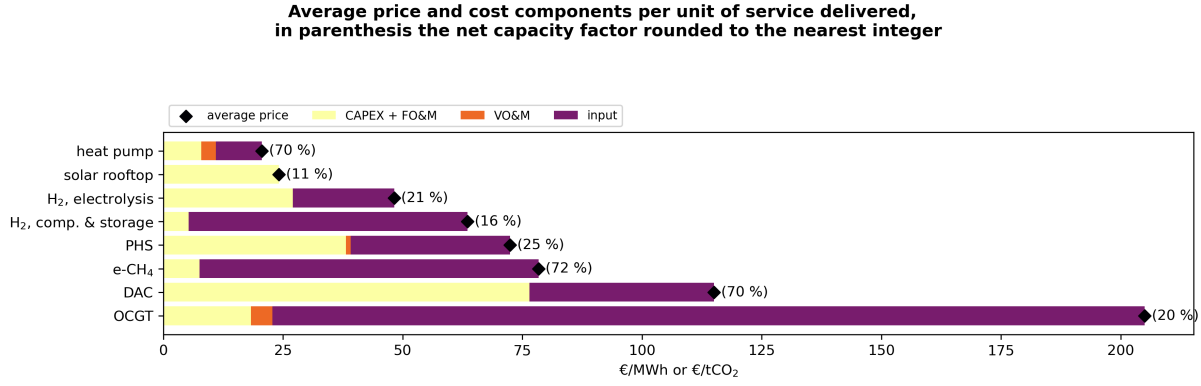


Figure 48: Scenario \dot{A} , technology-specific discount rates, vetoes on land-based renewables and nuclear, solar rooftop with low CF as in scenario C, average price and cost structure.

5.4 Results of scenarios for auxiliaries and a synthesis of the main vetoes

Figs. 49—52 report the main results of scenario \dot{A}_b with the same structure discussed for the previously presented scenarios. Figs. 53-54 provide additional results commented in the following. We observe that the LCOS of scenario \dot{A}_b is similar to that of scenario \dot{A} in the approximation of 1 euro/MWh, and thus, the improvement offered by biogenic gases at the given price levels is marginal. The deployment of the biogenic gases at the assumed prices can be regarded as a small variation around cost optimality. However, the sizing effects of the deployed technologies are not insignificant. Comparing the results of scenarios \dot{A}_b and \dot{A} , we observe the following three main advantages of biogenic gases. First, DAC is no longer deployed and is replaced by the supply of biogenic CO₂. Second, e-CH₄ is reduced, although not eliminated. Third, onshore wind and GPV installed capacities are reduced. Overall, scenario \dot{A}_b streamlines the optimal configuration, which can be appreciated by the cost-revenue balance of Fig. 53. The hourly inputs and the main indices of the methanation plant are illustrated in Fig. 54, to be compared with those of scenario A in Fig. 10. Biogenic gases reduce by a factor three the annual output of the methanation plant and significantly smooth out its operations.

Results of scenarios \dot{A}_p , \dot{A}_m and $\dot{A}_{p,m}$ are briefly commented in the following (full

details at the Git-Hub repository). In scenario \dot{A}_p , vetoing PHS yields a 5 €/MWh LCOS increase relative to scenario \dot{A} . Li-ion batteries take the role of PHS and are sized with 8 hours discharge. A small quantity of hydrogen is used in fuel cells. In scenario \dot{A}_m , methanation is constrained to zero, and its long-term storage role is taken by PHS and a small quantity of hydrogen. PHS is sized with a maximum discharge of 26 hours, approximately double the scenarios with methanation. The LCOS increase of this scenario relative to scenario \dot{A} is 4 €/MWh. In scenario $\dot{A}_{p,m}$, renouncing both PHS and methanation increases LCOS by 9 €/MWh relative to scenario \dot{A} . This is the only scenario where fuel cells play a significant role, covering 6% of the electricity demand.

We can now synthesize the extra costs induced by the main vetoes studied in this paper. Fig.55 illustrates the LCOS increases relative to scenario \dot{A} . Vetoes to land-based wind and solar have major impacts, and vetoes to PHS and methanation yield non-negligible effects. We observe that a veto to land-based wind and solar has an impact larger than the sum of the single-technology vetoes. This is not the case for auxiliary technologies where the combined veto is additive, i.e. a veto to both PHS and e-CH₄ is approximately equal to the sum of the two single vetoes. A veto on nuclear does not induce an extra cost.

5.5 Hydrogen competitiveness

It is unlikely that hydrogen at a cost higher than 1.5 €/kg would be competitive for industrial applications in the year 2050. Scenarios \dot{A} and A, with land-based wind and solar in a single district, may yield a *Levelized Cost of Hydrogen* (LCOH) of ~1 and 1.4 €/kg, respectively. Scenario G, only nuclear, leads to a LCOH of ~4 €/kg. A similar result occurs in scenario \dot{G} where the low discount rate assumption applies only to electrolysis, a small part of the total cost, and thus, it does not yield a significant impact in terms of LCOH reduction. Scenarios \dot{H} and H, solar rooftop only, allow smaller LCOH than exclusive nuclear, ~2.3 and 3.4 €/kg, respectively, but larger than the threshold for industrial competitiveness. In the scenario set with technology-specific discount rates, the only other scenario where the LCOH is smaller than 1.5 €/kg is scenario \dot{B} ,

**Primary generation, delivered electricity, and LCOS values and shares at 0 gCO₂/kWh, curtailment 1.3%, CO₂ shadow price 105 €/t
Delivered 8.76 TWh/y of electricity at 34.2 €/MWh and 2.19 TWh/y of H₂ at 32.8 €/MWh = 0.99 €/kg**

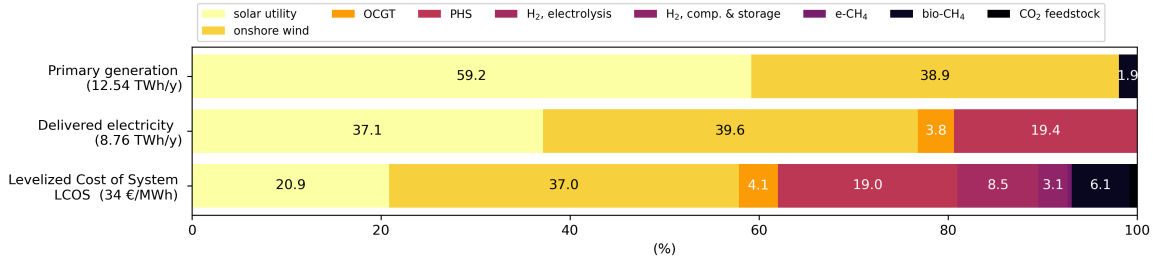


Figure 49: Scenario \dot{A}_b , technology-specific discount rates, with bio-gases, no vetoes, main indices.

where onshore wind is activated and solar rooftop replaces GPV but still strives for a high CF. In synthesis, South Italy has reasonable chances of hydrogen industrial production and use if and only if wind and solar are concomitantly deployed with high capacity factors.

Regarding the above comparison between nuclear and renewable-based hydrogen, two *caveats* hint that our cost gap is optimistic for nuclear. First, as reported in Section 3, the technical life of the electrolyser has been set to 20 years when its CF is 57%. Nuclear uses the electrolyser at its maximum CF of 90%, see Fig. 34. We did not iterate seeking convergence on this parameter, so we underestimated the CAPEX component of nuclear hydrogen. In scenarios \dot{A} and A, the electrolyser CFs are 49 and 46%, respectively. Therefore, the CAPEX component of the renewable-based hydrogen is overestimated for the lower CFs than assumed in the technical life. For an example of an iterative procedure for technical life convergence in system cost minimization, see Shirizadeh and Quirion (2023). Second, the single-district assumption is a significant limitation for renewable-based hydrogen since higher electrolyser CFs would be possible with wide-area transmission.

Given this, we conclude that the competitiveness of nuclear-based hydrogen would require a factor three LCOE reduction for this technology relative to our already optimistic 2050 assumptions. This conclusion can be appreciated by the cost structure of nuclear-based hydrogen reported in Fig. 34.

Installed capacities:
power or mass flow (top axis, linear scale)
and energy or mass (bottom axis, log scale,
and in parenthesis the maximum discharge duration in hours, rounded to the nearest integer)

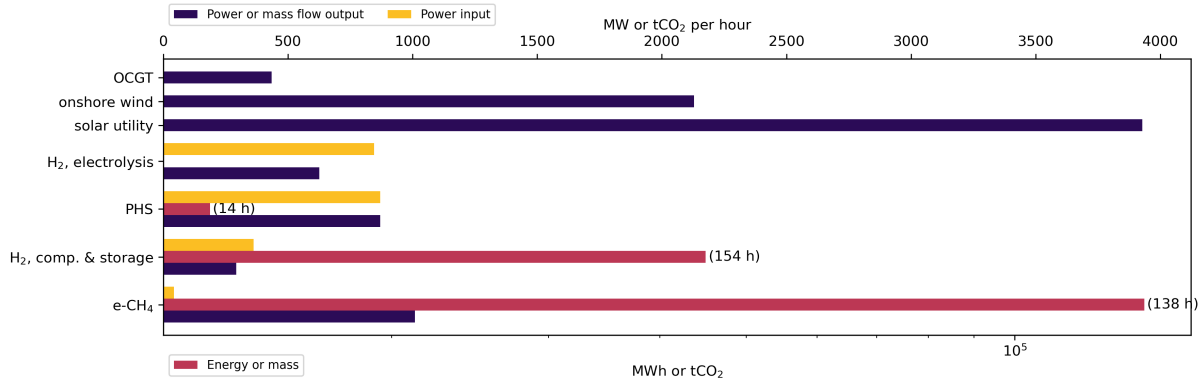


Figure 50: Scenario \dot{A}_b , technology-specific discount rates, with bio-gases, no vetoes, installed capacities.

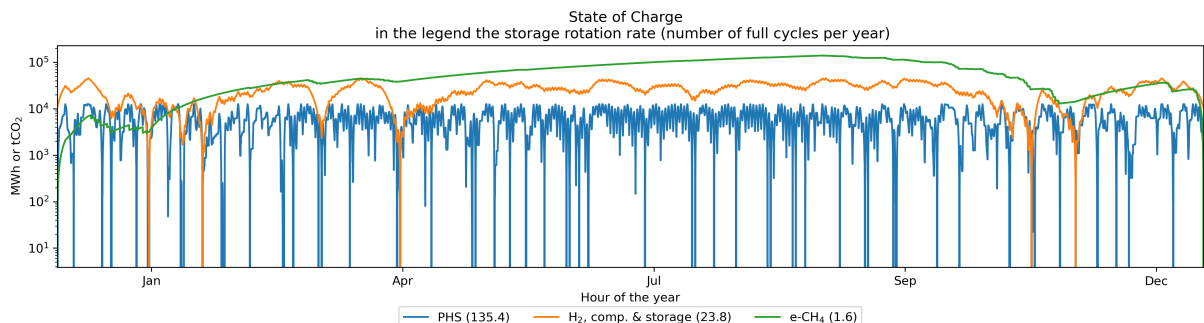


Figure 51: Scenario \dot{A}_b , technology-specific discount rates, with bio-gases, no vetoes, state of charge of storage.

Average price and cost components per unit of service delivered,
in parenthesis the net capacity factor rounded to the nearest integer

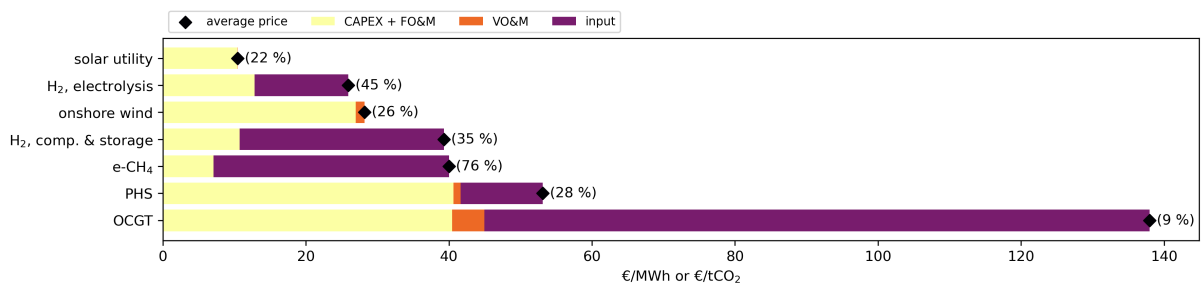


Figure 52: Scenario \dot{A}_b , technology-specific discount rates, with bio-gases, no vetoes, average price and cost structure.

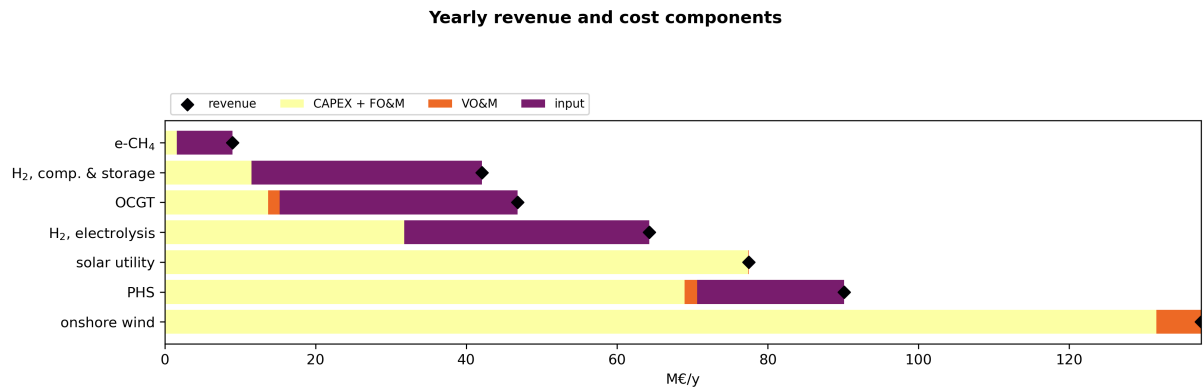


Figure 53: Scenario \dot{A}_b , technology-specific discount rates, with bio-gases, no vetoes, annual cost and revenues balances of the district sub-systems.

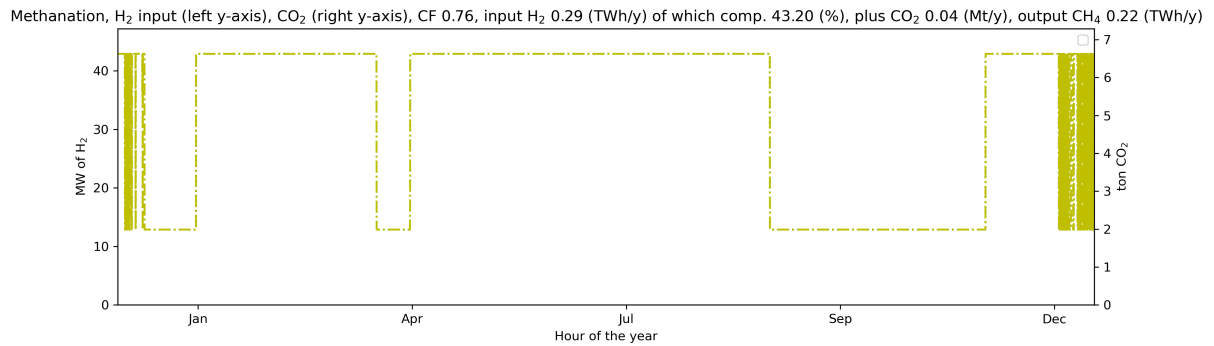


Figure 54: Scenario \dot{A}_b , technology-specific discount rates, with biogenic gases, no vetoes, main indices and hourly capacity factors of the methanation plant.

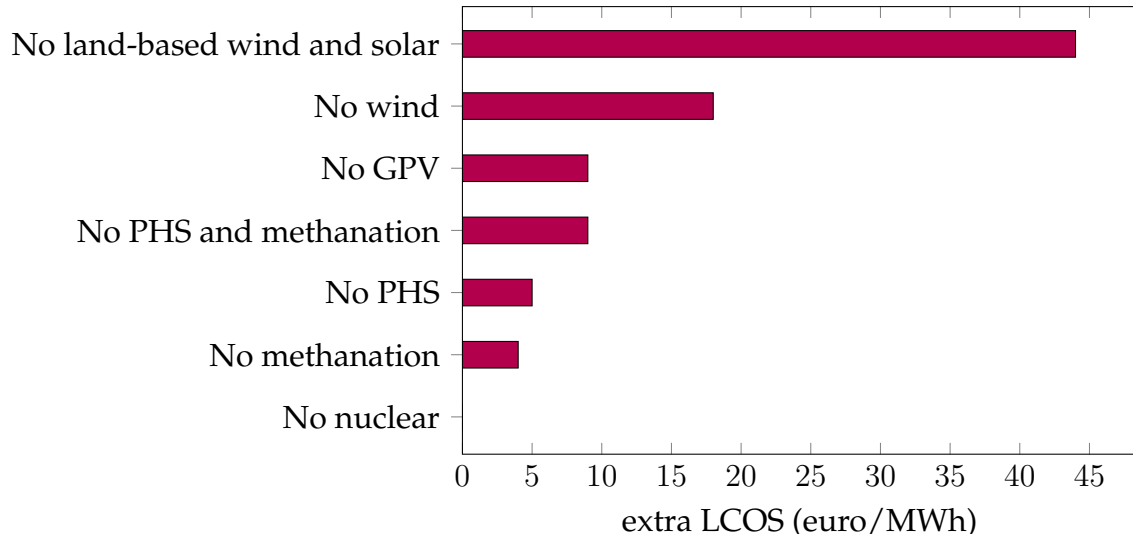


Figure 55: Increase of Levelized Cost of System relative to scenario \dot{A}

5.6 Geological storage of e-CH₄ in Italy

Geological storage of fossil gas in Italy amounts to 200 TWh_{th} (GIE, 2024). In scenarios A and \dot{A} , with land-based wind and solar, a nuclear-sized district in South Italy would require 0.25 TWh_{th} of storage capacity for e-CH₄. If all Italian baseload energy services in 2050 (400 TWh_e of electricity and 100 TWh_{th} of hydrogen⁴) would be supplied by such districts, 46 of them would be required. Their geological storage capacity of e-CH₄ would amount to ~6% of the existing capacity. If synergies with biogenic gases are pursued, scenario \dot{A}_b , the required storage capacity of e-CH₄ would halve. Additional factors could both reduce and increase the need for long-term storage capacity in the form of gas. Multi-year variability of wind and solar and strategic reserves for geopolitical crises could increase storage capacity. Conversely, cheaper seasonal storage, such as heat for district heating, may reduce it. Overall, our results point to long-term storage in Italy as unproblematic if methanation is pursued.

6 Conclusions and future work

We have presented an optimization model for baseload electricity and hydrogen services where decarbonization can be obtained by nuclear and renewable sources. We have defined several scenarios for 2050 to explore the system effects of discount rate sensitivity and vetoes on technologies. The scenarios address the following issues relevant for decarbonization in South Italy: land-based wind and solar *versus* exclusive solar rooftop, extra cost of a veto on nuclear, conservative assumptions on future storage technology and the role of PHS, lack of low-cost geological storage of hydrogen and the industrial competitiveness of this carrier, and the methanation synergy with the agro-forestry sector. The model's code, data, and results are available at the GitHub repository Moccia (2024) for transparency and replicability.

Our results quantify the high system cost of vetoes on land-based wind and solar. Exclusive solar rooftop causes severe overgeneration, and life-cycle environmental

⁴Our hypotheses, see Peschi et al. (2021) for 2050 decarbonization scenarios for Italy.

impacts may more than double relative to the optimal mix of land-based wind and solar. Nuclear may enter the optimal mix only with a veto against onshore wind and a hypothesis of equal project risk, hence an equal discount rate, with renewables. With a realistic gap in discount rates between nuclear and renewables, a veto on the former technology does not yield an extra cost. In scenarios without vetoes to land-based wind and solar, PHS is the main storage technology and allows the renewables to supply ~97% of the electricity demand at a low average cost. This result shows that criticism of renewable-based energy systems for expensive storage is unfounded. Scenarios with land-based wind and solar obtain low-cost hydrogen and hence allow industrial uses of this carrier. Both nuclear and exclusive solar rooftop fail this target. The methanation synergy with the agro-forestry sector does not offer a system cost advantage relative to DAC. Still, it improves the configuration of the district by halving the storage requirement of synthetic methane, smoothing the utilization factor of the methanation plant, and reducing the installed capacities of wind and solar. Long-term storage via synthetic methane allows districts with land-based wind and solar to supply baseload electricity and hydrogen with 100% decarbonization at low cost, using only a small fraction of the existing infrastructure for geological storage of fossil gas. Analysis of the shadow prices shows that the minimum cost configuration ensures the cost-revenue balance of each sub-system in the district. The extra cost of full decarbonization relative to unregulated fossil gas is small with land-based wind and solar but very significant when vetoes to these technologies apply. Scenarios with time-varying electricity yield comparable main indices relative to the main scenarios studied in this paper with baseload electricity, hence, our results may offer insights for more general cases.

Future work may address sizing transmission networks of electricity and hydrogen in Italy, where nodes are districts modeled as in this paper. By so doing, national scenarios could be explored, and the advantage of wide-area renewable diversity *versus* transmission could be assessed.

Acknowledgments

This work would not have been possible without the community of open-source modelers who have shared their knowledge in such a granular and transparent way. Partial support has been provided by the European Union under project PNNR-FAIR, topic Green AI. The author is also grateful to Sandra Gagné for proofreading assistance.

A Scenarios with time-varying demand of electricity

The results derived from the optimization of baseload energy services, as in our main scenarios, are relevant for the more general case when demand is time-varying, for example by an hourly profile? To quantitatively answer this question, we define a new set of scenarios indicated by \tilde{A} — \tilde{H} . These scenarios inherit characteristics of scenarios A—H with the following two modifications. First, in scenarios \tilde{A} — \tilde{H} electricity demand has a time-varying profile derived from 2015 consumption data in Italy. This demand profile is scaled such that the annual demand is 8.76 TWh, thus equal to that of the main scenarios. Second, hydrogen demand is assumed as baseload and set to 0.15 GW instead of 0.25 GW as in our main scenarios. These two assumptions on the hydrogen demand are motivated in the following. First, a baseload demand of hydrogen is the more realistic scenario for the industrial uses of this energy carrier, and therefore, we have maintained this assumption in the new scenarios \tilde{A} — \tilde{H} . Second, regarding the scaling down of the hydrogen demand, we observe that in our main scenarios the hydrogen demand is set to 25% of the electricity demand to attain 100 TWh_{th}/y when 46 districts are deployed in Italy. By so doing, the baseload electricity supplied by these 46 districts would be 400 TWh_e/y. These values are in the range of 2050 energy scenarios for Italy. The districts modeled by scenarios \tilde{A} — \tilde{H} are instead sub-units of the total electric demand that in 2050 may reach 700 TWh_e/y. Maintaining the target of 100 TWh_{th}/y for hydrogen implies a reduction of the hydrogen share at the single-district level. Thus, a district modeled by scenarios \tilde{A} — \tilde{H} is 1/80 of the whole Italian electricity-hydrogen system in 2050.

Scenario	Solar utility	Solar rooftop high CF	Solar rooftop low CF	Onshore wind	Nuclear
\tilde{A}	✓62	○	○	✓38	○
\tilde{B}	✗	✓61	○	✓39	○
\tilde{C}	✗	✗	✓51	✓49	○
\tilde{D}	✓79	○	○	✗	✓21
\tilde{E}	✗	✓56	○	✗	✓44
\tilde{F}	✗	✗	✓24	✗	✓76
\tilde{G}	✗	✗	✗	✗	✓100
\tilde{H}	✗	✗	✓100	✗	✗

Table 4: Synthesis of vetoes and shares of primary technologies in scenarios \tilde{A} — \tilde{H} . A vetoed technology is indicated by \times . The symbol \circ designates a technology that, although not vetoed in a scenario, it is not activated for lack of competitiveness. A technology that is activated is reported by the symbol ✓with its percentage in the primary generation (rounded to the nearest integer).

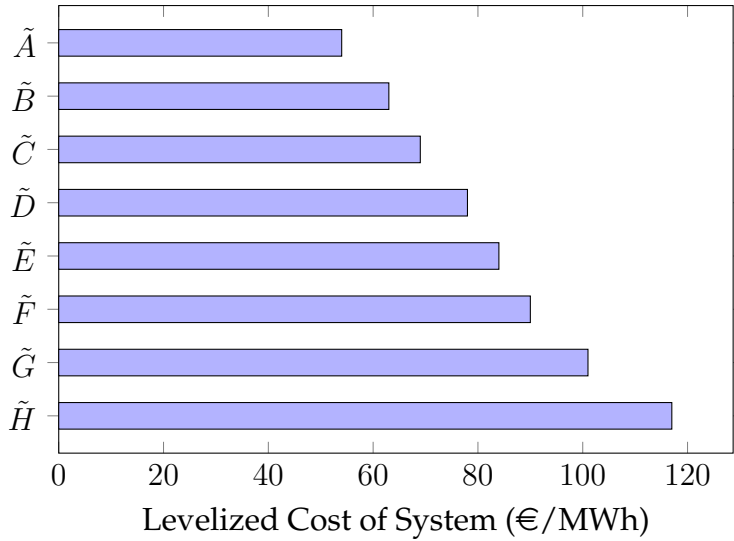


Figure 56: Levelized Cost of System of scenarios \tilde{A} — \tilde{H}

For synthesis, we do not include in this paper all results for scenarios \tilde{A} — \tilde{H} (full results are available at the Git-Hub repository Moccia (2024)). Tab. 4 and Fig. 56 report the technology vetoes and primary shares, and LCOS of scenarios \tilde{A} — \tilde{H} , respectively. Comparing these results with those of scenarios A—H, Tab. 2 and Fig. 39, allows us to conclude that the differences between baseload and time-varying electricity demands are small in terms of system cost and technology primary shares.

B Scenarios with unconstrained CO₂

This appendix shows how our model can quantify the regulation gap of full decarbonization under technology vetoes. We define new scenarios indicated as \dot{A}_f — \dot{H}_f derived from scenarios \dot{A} — \dot{H} with the following three modifications. First, we relax the full decarbonization constraint by setting an upper bound for the CO₂ emissions. By so doing, fossil gas can be deployed at the CH₄ bus and supply OCGT. Second, we add another power technology between the CH₄ and electricity buses, namely the *Combined Cycle Gas Turbine* (CCGT). This technology uses fossil gas more efficiently relative to OCGT, albeit with a higher capital cost. The system optimization deals with the pros and cons of higher fuel efficiency *vs.* higher CAPEX. Adding CCGT ensures that fossil gas is assessed under realistic competitive assumptions. Third, we remove the hydrogen demand from the model. Without a full decarbonization constraint on the electricity sector it is unlikely that other sectors will demand a carrier such as hydrogen. Moreover, without an explicit constraint on CO₂ emissions we could produce hydrogen from electricity generated from fossil gas, which would not make any economic or environmental sense. Thus, the results of these new scenarios represent the electricity sector with unregulated CO₂.

The complete set of results for scenarios \dot{A}_f — \dot{H}_f is available at the Git-Hub repository Moccia (2024). Tab. 5 reports the vetoes and primary shares of technologies and fossil gas. Full decarbonization is not attained in any scenario. The primary share of fossil gas has its minimum in scenario \dot{A}_f , where land-based wind and solar are allowed, and its maximum of 100% in scenario \dot{G}_f , where all renewables are vetoed and the only carbon-free technology would have been nuclear if competitive, which is not the case. Scenarios \dot{A}_f and \dot{G}_f are also those where the electricity cost attains the minimum (32 €/MWh) and maximum (46 €/MWh) value, respectively. The cost spread in these scenarios is not large, but these costs need to be compared with those of scenarios \dot{A} — \dot{H} to assess the effect of full decarbonization. For example, the electricity cost of scenario \dot{A} is only 3 €/MWh larger than in scenario \dot{A}_f . Thus the extra cost of full decarbonization when land-based wind and solar are allowed is small. Instead, the

Scenario	Solar utility	Solar rooftop high CF	Solar rooftop low CF	Onshore wind	Nuclear	Fossil gas
\dot{A}_f	✓52	○	○	✓32	○	✓16
\dot{B}_f	✗	✓31	○	✓40	○	✓29
\dot{C}_f	✗	✗	✓24	✓42	○	✓34
\dot{D}_f	✓46	○	○	✗	○	✓54
\dot{E}_f	✗	✓30	○	✗	○	✓70
\dot{F}_f	✗	✗	✓26	✗	○	✓74
\dot{G}_f	✗	✗	✗	✗	○	✓100
\dot{H}_f	✗	✗	✓26	✗	✗	✓74

Table 5: Synthesis of vetoes and shares of primary technologies and fuel in scenarios \dot{A}_f — \dot{H}_f . A vetoed technology is indicated by ✗. The symbol ○ designates a technology that, although not vetoed in a scenario, it is not activated for lack of competitiveness. A technology that is activated is reported by the symbol ✓with its percentage in the primary generation (rounded to the nearest integer).

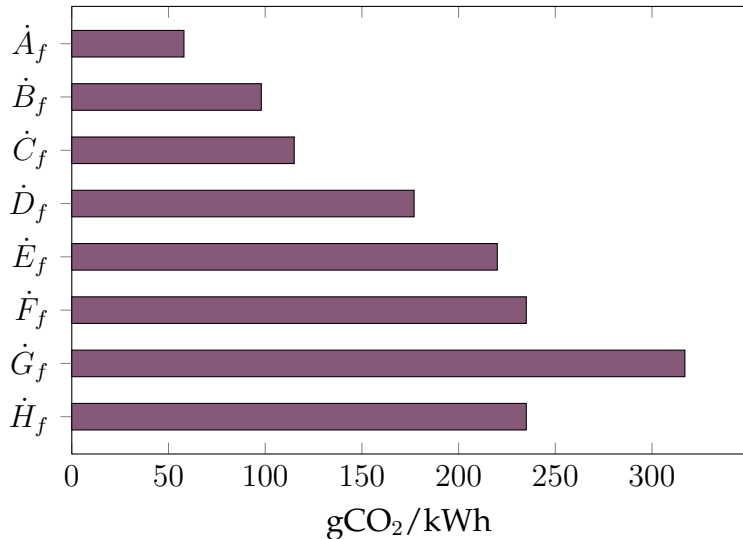


Figure 57: Electricity emission factor of scenarios \dot{A}_f — \dot{H}_f

electricity cost of scenario \dot{H} is 37 €/MWh larger than in scenario \dot{H}_f , casting doubts on the socio-economical feasibility of full decarbonization under generalized vetoes. We observe that nuclear is never competitive in these scenarios with unconstrained CO₂. Moreover, vetoing renewables in order to favor nuclear yields scenario \dot{G}_f , the costlier and more polluting scenario, see Fig. 57 that illustrates the electricity emission factor of CO₂ in this scenario set.

References

- ADEME (2018). Un mix de gaz 100% renouvelable en 2050? Technical report, Agence de l'environnement et de la maîtrise de l'énergie, Angers, France.
- Afanasyeva, S., Bogdanov, D., and Breyer, C. (2018). Relevance of pv with single-axis tracking for energy scenarios. *Solar Energy*, 173:173–191.
- Aghahosseini, A. and Breyer, C. (2018). Assessment of geological resource potential for compressed air energy storage in global electricity supply. *Energy Conversion and Management*, 169:161–173.
- Agora Energiewende (2018). The future cost of electricity-based synthetic fuels. Technical report, Agora Energiewende, Berlin.
- Armstrong, A., Brown, L., Davies, G., Whyatt, J. D., and Potts, S. G. (2021). Honeybee pollination benefits could inform solar park business cases, planning decisions and environmental sustainability targets. *Biological Conservation*, 263:109332.
- Barison, E., Donda, F., Merson, B., Le Gallo, Y., and Réveillère, A. (2023). An insight into underground hydrogen storage in Italy. *Sustainability*, 15(8).
- Blanco, H. and Faaij, A. (2018). A review at the role of storage in energy systems with a focus on power to gas and long-term storage. *Renewable and Sustainable Energy Reviews*, 81:1049–1086.
- Bouckaert, S., Pales, A. F., McGlade, C., Remme, U., Wanner, B., Varro, L., D'Ambrosio, D., and Spencer, T. (2021). Net zero by 2050: A roadmap for the global energy sector. Technical report, International Energy Agency, Paris, France.
- Breyer, C., Khalili, S., Bogdanov, D., Ram, M., Oyewo, A. S., Aghahosseini, A., Gulagi, A., Solomon, A. A., Keiner, D., Lopez, G., Østergaard, P. A., Lund, H., Mathiesen, B. V., Jacobson, M. Z., Victoria, M., Teske, S., Pregger, T., Fthenakis, V., Raugei, M., Holttinen, H., Bardi, U., Hoekstra, A., and Sovacool, B. K. (2022). On the history and future of 100% renewable energy systems research. *IEEE Access*, 10:78176–78218.

- Brown, T. and Reichenberg, L. (2021). Decreasing market value of variable renewables can be avoided by policy action. *Energy Economics*, 100:105354.
- Caglayan, D. G., Weber, N., Heinrichs, H. U., Linßen, J., Robinius, M., Kukla, P. A., and Stolten, D. (2020). Technical potential of salt caverns for hydrogen storage in Europe. *International Journal of Hydrogen Energy*, 45(11):6793–6805.
- Carbone, C., Gracceva, F., Pierro, N., Motola, V., Zong, Y., You, S., Pérez-Fortes, M., Wang, L., and Agostini, A. (2021). Potential deployment of reversible solid-oxide cell systems to valorise organic waste, balance the power grid and produce renewable methane: A case study in the southern Italian peninsula. *Frontiers in Energy Research*, 9:1–17.
- Connolly, D., Lund, H., and Mathiesen, B. V. (2016). Smart energy Europe: The technical and economic impact of one potential 100% renewable energy scenario for the European Union. *Renewable and Sustainable Energy Reviews*, 60:1634–1653.
- Crameri, F., Shephard, G. E., and Heron, P. J. (2020). The misuse of colour in science communication. *Nature communications*, 11(1):5444
- Danelli, A. and Brivio, E. (2021). Analisi LCA di un impianto fotovoltaico piano con moduli PERC e confronto con altre tecnologie innovative. Technical report, Ricerca sul Sistema Energetico (RSE), Milano, Italy.
- DEA (2022a). Technology data for carbon capture, transport and storage. Technical report, Danish Energy Agency, Copenhagen, Denmark.
- DEA (2022b). Technology data for industrial process heat. Technical report, Danish Energy Agency, Copenhagen, Denmark.
- DEA (2022c). Technology data for power and heat production plants. Technical report, Danish Energy Agency, Copenhagen, Denmark.
- Fanelli, M., Faggian, P., Frigerio, A., and Mazzà, G. (2018). Gestione integrata delle crisi idriche — il ruolo delle interconnessioni idriche a lungo raggio. *L'Acqua*, (6):19–28.

Fasihi, M. and Breyer, C. (2020). Baseload electricity and hydrogen supply based on hybrid pv-wind power plants. *Journal of Cleaner Production*, 243:118466.

Flyvbjerg, B. (2017). *The Oxford handbook of megaproject management*. Oxford University Press, Oxford, UK.

Frigerio, A., Meghella, M., and Bruno, G. (2012). Valutazione del potenziale dei sistemi di accumulo di energia mediante centrali di pompaggio idroelettrico per il sistema idroelettrico italiano – analisi di fattibilità preliminari. Technical report, RSE - Ricerca Sistema Energetico, Milano, Italy.

GIE (2024). AGSI storage inventory. <https://agsi.gie.eu/>.

GSE (2022). Rapporto statistico solare fotovoltaico 2021. Technical report, Gestore dei Servizi Energetici S.p.A., Roma, Italy.

Guerra, O. J., Eichman, J., and Denholm, P. (2021). Optimal energy storage portfolio for high and ultrahigh carbon-free and renewable power systems. *Energy & Environmental Science*, 14(10):5132–5146.

Haywood, L., Leroutier, M., and Pietzcker, R. (2023). Why investing in new nuclear plants is bad for the climate. *Joule*, 7(8):1675–1678.

Hofmann, F., Hampp, J., Neumann, F., Brown, T., and Hörsch, J. (2021). Atlite: a lightweight python package for calculating renewable power potentials and time series. *Journal of Open Source Software*, 6(62):3294.

Hörsch, J., Hofmann, F., Schlachtberger, D., and Brown, T. (2018). Pypsa-eur: An open optimisation model of the european transmission system. *Energy strategy reviews*, 22:207–215.

IEA (2019). The future of hydrogen — assumptions annex. Technical report, International Energy Agency, Paris, France.

Jacobson, M. Z. (2020). *100% clean, renewable energy and storage for everything*. Cambridge University Press, Cambridge, UK.

Jacobson, M. Z., von Krauland, A.-K., Coughlin, S. J., Dukas, E., Nelson, A. J. H., Palmer, F. C., and Rasmussen, K. R. (2022). Low-cost solutions to global warming, air pollution, and energy insecurity for 145 countries. *Energy & Environmental Science*, 15(8):3343–3359.

Jurasz, J., Canales, F. A., Kies, A., Guezgouz, M., and Beluco, A. (2020). A review on the complementarity of renewable energy sources: Concept, metrics, application and future research directions. *Solar Energy*, 195:703–724.

Korberg, A. D., Mathiesen, B. V., Clausen, L. R., and Skov, I. R. (2021). The role of biomass gasification in low-carbon energy and transport systems. *Smart Energy*, 1:100006.

Lantz, E. J., Roberts, J. O., Nunemaker, J., DeMeo, E., Dykes, K. L., and Scott, G. N. (2019). Increasing wind turbine tower heights: Opportunities and challenges. Technical report, National Renewable Energy Laboratory (NREL), Golden, CO, US.

Lauri, K., Jouko, R., Nicklas, N., and Sebastian, T. (2014). Scenarios and new technologies for a north-european CO₂ transport infrastructure in 2050. *Energy Procedia*, 63:2738–2756.

Lazard (2019). Levelized cost of energy analysis.

Lombardi, F., Pickering, B., Colombo, E., and Pfenninger, S. (2020). Policy decision support for renewables deployment through spatially explicit practically optimal alternatives. *Joule*, 4(10):2185–2207.

Lu, B., Stocks, M., Blakers, A., and Anderson, K. (2018). Geographic information system algorithms to locate prospective sites for pumped hydro energy storage. *Applied Energy*, 222:300–312.

Lund, H., Østergaard, P. A., Connolly, D., Ridjan, I., Mathiesen, B. V., Hvelplund, F., Thellufsen, J. Z., and Sorknæs, P. (2016). Energy storage and smart energy systems. *International Journal of Sustainable Energy Planning and Management*, 11(0):3–14.

Lund, H., Østergaard, P. A., Nielsen, T. B., Werner, S., Thorsen, J. E., Gudmundsson, O., Arabkoohsar, A., and Mathiesen, B. V. (2021). Perspectives on fourth and fifth generation district heating. *Energy*, 227:120520.

Macknick, J., Beatty, B., and Hill, G. (2013). Overview of opportunities for co-location of solar energy technologies and vegetation. Technical report, National Renewable Energy Laboratory (NREL), Golden, CO, US.

Mathiesen, B. V., Lund, H., Connolly, D., Wenzel, H., Østergaard, P. A., Möller, B., Nielsen, S., Ridjan, I., Karnøe, P., Sperling, K., and Hvelplund, F. K. (2015). Smart energy systems for coherent 100% renewable energy and transport solutions. *Applied Energy*, 145:139–154.

Miglietta, M. M., Huld, T., and Monforti-Ferrario, F. (2017). Local complementarity of wind and solar energy resources over europe: An assessment study from a meteorological perspective. *Journal of Applied Meteorology and Climatology*, 56(1):217–234.

Moccia, L. (2024). Nuclear-sized energy district to assess renewable and storage technologies. https://github.com/luigimoccia/single_district.

Möller, B., Wiechers, E., Persson, U., Grundahl, L., Lund, R. S., and Mathiesen, B. V. (2019). Heat roadmap europe: Towards eu-wide, local heat supply strategies. *Energy*, 177:554–564.

MONTEL (2024). Nuclear to make up 10pc of italy's energy mix by 2040 – ministry. <https://montelnews.com/news/c5b30714-0e0d-43c7-9e78-4fd636119561/nuclear-to-make-up-10-of-italys-mix-by-2040-ministry>.

Morrison, R. (2018). Energy system modeling: Public transparency, scientific reproducibility, and open development. *Energy Strategy Reviews*, 20:49–63.

Mortensen, A. W., Mathiesen, B. V., Hansen, A. B., Pedersen, S. L., Grandal, R. D., and Wenzel, H. (2020). The role of electrification and hydrogen in breaking the biomass

- bottleneck of the renewable energy system –a study on the danish energy system. *Applied Energy*, 275:115331.
- Neumann, F. and Brown, T. (2021). The near-optimal feasible space of a renewable power system model. *Electric Power Systems Research*, 190:106690.
- Neumann, F., Zeyen, E., Victoria, M., and Brown, T. (2023). The potential role of a hydrogen network in europe. *Joule*, 7(8):1793–1817.
- Nyenah, E., Sterl, S., and Thiery, W. (2022). Pieces of a puzzle: solar-wind power synergies on seasonal and diurnal timescales tend to be excellent worldwide. *Environmental Research Communications*, 4(5):055011.
- Paardekooper, S., Lund, H., Thellufsen, J. Z., Bertelsen, N., and Mathiesen, B. V. (2022). Heat roadmap europe: strategic heating transition typology as a basis for policy recommendations. *Energy Efficiency*, 15(5):32.
- Pelser, T., Weinand, J. M., Kuckertz, P., McKenna, R., Linssen, J., and Stolten, D. (2024). Reviewing accuracy & reproducibility of large-scale wind resource assessments. *Advances in Applied Energy*, 13:100158.
- Peschi, E., Caputo, A., Di Cristofaro, E., Colaiezzi, M., Pantaleoni, M., Vitullo, M., and Gaeta, M. (2021). La strategia italiana di lungo termine sulla riduzione delle emissioni di gas serra: Scenari emissivi e trend storici. *Ingegneria dell'Ambiente*, 8(3).
- Pfenninger, S. and Staffell, I. (2016). Long-term patterns of european pv output using 30 years of validated hourly reanalysis and satellite data. *Energy*, 114:1251–1265.
- Pierro, N., Giocoli, A., De Bari, I., Agostini, A., Motola, V., and Dipinto, S. (2021). Potenziale teorico di biometano avanzato in italia. Technical report, ENEA, Roma, Italy.
- Raugei, M., Frischknecht, R., Olson, C., Sinha, P., and Heath, G. (2021). Methodological guidelines on net energy analysis of photovoltaic electricity, IEA-PVPS Task 12, re-

port t12-20: 2021. Technical Report T12-20, International Energy Agency - IEA-PVPS Task 12, Paris, France.

Rinne, E., Holttinen, H., Kiviluoma, J., and Rissanen, S. (2018). Effects of turbine technology and land use on wind power resource potential. *Nature Energy*, 3(6):494–500.

Ryberg, D., Robinius, M., and Stolten, D. (2018). Evaluating Land Eligibility Constraints of Renewable Energy Sources in Europe. *Energies*, 11(5):1246.

Ryberg, D. S., Caglayan, D. G., Schmitt, S., Linßen, J., Stolten, D., and Robinius, M. (2019). The future of european onshore wind energy potential: Detailed distribution and simulation of advanced turbine designs. *Energy*, 182:1222–1238.

Ryberg, D. S., Tulemat, Z., Stolten, D., and Robinius, M. (2020). Uniformly constrained land eligibility for onshore european wind power. *Renewable Energy*, 146:921–931.

Satymov, R., Bogdanov, D., and Breyer, C. (2022). Global-local analysis of cost-optimal onshore wind turbine configurations considering wind classes and hub heights. *Energy*, 256:124629.

Schlachtberger, D. P., Brown, T., Schäfer, M., Schramm, S., and Greiner, M. (2018). Cost optimal scenarios of a future highly renewable european electricity system: Exploring the influence of weather data, cost parameters and policy constraints. *Energy*, 163:100–114.

Schlachtberger, D. P., Brown, T., Schramm, S., and Greiner, M. (2017). The benefits of cooperation in a highly renewable european electricity network. *Energy*, 134:469–481.

Semeraro, T., Aretano, R., Barca, A., Pomes, A., Del Giudice, C., Gatto, E., Lenucci, M., Buccolieri, R., Emmanuel, R., Gao, Z., and Scognamiglio, A. (2020). A conceptual framework to design green infrastructure: Ecosystem services as an opportunity for creating shared value in ground photovoltaic systems. *Land*, 9(8).

- Semeraro, T., Aretano, R., Barca, A., Pomes, A., Del Giudice, C., Lenucci, M., and Scognamiglio, A. (2022a). Transfer of ecology approach in ground photovoltaic engineering design to support ecosystem services like water supply. In Heggy, E., Bermudez, V., and Vermeersch, M., editors, *Sustainable Energy-Water-Environment Nexus in Deserts*, pages 509–519, Berlin, Germany. Springer.
- Semeraro, T., Pomes, A., Del Giudice, C., Negro, D., and Aretano, R. (2018). Planning ground based utility scale solar energy as green infrastructure to enhance ecosystem services. *Energy Policy*, 117:218–227.
- Semeraro, T., Scarano, A., Santino, A., Emmanuel, R., and Lenucci, M. (2022b). An innovative approach to combine solar photovoltaic gardens with agricultural production and ecosystem services. *Ecosystem Services*, 56:101450.
- Shirizadeh, B., Perrier, Q., and Quirion, P. (2022). How sensitive are optimal fully renewable power systems to technology cost uncertainty? *The Energy Journal*, 43(1):43–75.
- Shirizadeh, B. and Quirion, P. (2021). Low-carbon options for the french power sector: What role for renewables, nuclear energy and carbon capture and storage? *Energy Economics*, 95:105004.
- Shirizadeh, B. and Quirion, P. (2022). The importance of renewable gas in achieving carbon-neutrality: Insights from an energy system optimization model. *Energy*, 255:124503.
- Shirizadeh, B. and Quirion, P. (2023). Long-term optimization of the hydrogen-electricity nexus in france: Green, blue, or pink hydrogen? *Energy Policy*, 181:113702.
- Simon, T. R., Inman, D., Hanes, R., Avery, G., Hettinger, D., and Heath, G. (2023). Life cycle assessment of closed-loop pumped storage hydropower in the United States. *Environmental Science & Technology*, 57(33):12251–12258.
- Staffell, I. and Pfenninger, S. (2016). Using bias-corrected reanalysis to simulate current and future wind power output. *Energy*, 114:1224–1239.

- Stöckl, F., Schill, W.-P., and Zerrahn, A. (2021). Optimal supply chains and power sector benefits of green hydrogen. *Scientific Reports*, 11(1):14191.
- Stocks, M., Stocks, R., Lu, B., Cheng, C., and Blakers, A. (2021). Global atlas of closed-loop pumped hydro energy storage. *Joule*, 5(1):270–284.
- Takle, E. S. and Shaw, R. H. (1979). Complimentary nature of wind and solar energy at a continental mid-latitude station. *International Journal of Energy Research*, 3(2):103–112.
- TERNA-SNAM (2022). Documento di descrizione degli scenari 2022. Technical report, Terna, SNAM, Roma, Italy.
- Thellufsen, J. Z., Lund, H., Sorknæs, P., Nielsen, S., Chang, M., and Mathiesen, B. V. (2023). Beyond sector coupling: Utilizing energy grids in sector coupling to improve the european energy transition. *Smart Energy*, 12:100116.
- Tröndle, T., Lilliestam, J., Marelli, S., and Pfenninger, S. (2020). Trade-offs between geographic scale, cost, and infrastructure requirements for fully renewable electricity in Europe. *Joule*, 4(9):1929–1948.
- Victoria, M., Zhu, K., Brown, T., Andresen, G. B., and Greiner, M. (2019). The role of storage technologies throughout the decarbonisation of the sector-coupled european energy system. *Energy Conversion and Management*, 201:111977.
- Walston, L. J., Mishra, S. K., Hartmann, H. M., Hlohowskyj, I., McCall, J., and Macknick, J. (2018). Examining the potential for agricultural benefits from pollinator habitat at solar facilities in the United States. *Environmental Science & Technology*, 52(13):7566–7576.
- Wiser, R., Rand, J., Seel, J., Beiter, P., Baker, E., Lantz, E., and Gilman, P. (2021). Expert elicitation survey predicts 37% to 49% declines in wind energy costs by 2050. *Nature Energy*, 6(5):555–565.

Wohland, J., Brayshaw, D., and Pfenninger, S. (2021). Mitigating a century of european renewable variability with transmission and informed siting. *Environmental Research Letters*, 16(6):064026